A two-fluid hyperbolic model in a porous medium

Laëtitia Girault, Jean-Marc Hérard

A two-fluid hyperbolic model in a porous medium

Laëtitia Girault *
EDF, R&D

Jean-Marc Hérard†
EDF, R&D

The paper is devoted to the computation of two-phase flows in a porous medium when applying the two-fluid approach. The basic formulation is presented first, together with the main properties of the model. A few basic analytic solutions are then provided, some of them corresponding to solutions of the one-dimensional Riemann problem. Three distinct Finite-Volume schemes are then introduced. The first two schemes, which rely on the Rusanov scheme, are shown to give wrong approximations in some cases involving sharp porous profiles. The third one, which is an extension of a scheme proposed by D. Kröner and M. D. Thanh ([27]) for the computation of single phase flows in varying cross section ducts , provides fair results in all situations. Properties of schemes and numerical results are presented. Analytic tests enable to compute the L^1 norm of the error.

I. Introduction

The main purpose of the present work is to develop models and schemes that allow the computation of two-phase flows in a porous medium while focusing on the two-fluid approach, and thus considering distinct pressure, velocity and temperature fields within each phase. Following the pioneering work of Baer and Nunziatto[3] , Kapila et al[25] , and more recent work[8, 13] , that deals with the two-fluid two-pressure approach in an open medium, we first provide an extension to the framework of porous medium as proposed in [24] . As expected, the system is hyperbolic, at least for small enough Mach number within each phase, which of course seems reasonable when focusing on applications for flows in pressurised water reactors in nuclear power plants. The governing set of equations also benefits from two major features. Though it contains some non-conservative products, all jump conditions are unique in single genuinely non linear -GNL- fields. This is tightly connected with the fact that the closure law for the so-called interfacial velocity is such that the field associated with the eigenvalue $\lambda = V_I$ is linearly degenerated - LD- (see also[8]). Moreover, we emphasize that a relevant entropy inequality holds for regular solutions of the whole set of equations including source terms (and viscous terms if any).

Once the model is presented (section II), section III will provide some details on a few analytic solutions of the whole system that will be investigated in sections V and VI. We will then focus in section IV on three simple Finite Volume schemes in order to compute approximations of the latter model in a porous medium. The first scheme corresponds to the classical Rusanov scheme, the second one being a slight modification of the latter. The third scheme is quite different. It relies on former propositions by Greenberg and Leroux (see[20]) revisited by Kröner and Thanh (see[27] , and[4] too). Actually the latter third scheme does not require solving an exact Riemann problem around each cell interface (see [19]), and thus is much simpler than the original well-balanced scheme[20] . The main properties of the schemes will be given in section V, with special emphasis on the well-balanced properties of course, but also on positivity properties. The last two sections will be devoted to the presentation of numerical results. More precisely, section VI will give the opportunity to examine the convergence rate of the above mentionned schemes with respect to the mesh size. Eventually, we will focus in section VII on the computation of the interaction of moving waves with the standing free/porous interface. Beyond the present work, we would like to mention that we aim at investigating some possible way to ensure a relevant interfacial and unsteady coupling of existing codes associated with free and porous medium respectively. This motivates the numerical experiments that are introduced within the last

*PhD student, EDF, R&D, Fluid Dynamics, Power Generation and Environment, 6 quai Watier, 78400, Chatou, France. Also in: Centre de Mathématique et Informatique, LATP, 39 rue Joliot Curie, 13453, Marseille cedex 13, France

†EDF, R&D, Fluid Dynamics, Power Generation and Environment, 6 quai Watier, 78400, Chatou, France.

two sections. For a further insight on the interfacial coupling of models, we refer to the recent work by the working group[0] , and more precisely on the early work [17, 18] , but also to the recent review article[16] , and also on[5] .

II. A two-fluid model in a porous medium

We first need to present the two-fluid two-pressure model introduced in [24] , and we shall also recall some of its properties afterwards.

A. Governing equations for the two-fluid model

We first introduce the void fraction $\alpha_k \in [0,1]$ that complies with $\alpha_1 + \alpha_2 = 1$, the porosity $\epsilon \in]0,1]$, and (for $k = 1,2$) the mean velocity U_k, the mean pressure P_k, the mean density ρ_k, the internal energy $e_k = e_k(P_k, \rho_k)$ in phase k. The state variable W in $\mathbf{R}^8$ is:

$$W^t = (\epsilon, \alpha_2, \epsilon m_1, \epsilon m_2, \epsilon m_1 U_1, \epsilon m_2 U_2, \epsilon E_1, \epsilon E_2) \tag{1}$$

We will also use W_ϵ defined as follows:

$$W_\epsilon^t = (\epsilon m_k, \epsilon m_k U_k, \epsilon E_k) \tag{2}$$

in $\mathbf{R}^6$, while noting $m_k = \alpha_k \rho_k$ the partial mass in phase k, and $E_k = m_k U_k^2/2 + m_k e_k$ the total energy of phase k. The equation of state (EOS) is provided through the function $e_k(P_k, \rho_k)$, which may be arbitrary. We will thus focus herein on the following two-fluid model:

$$\left\{ \begin{array}{l} \partial_t(\epsilon) = 0 \ ; \\ \partial_t(\alpha_2) + V_I \partial_x(\alpha_2) = \phi_2(W) \ ; \\ \partial_t(\epsilon m_k) + \partial_x(\epsilon m_k U_k) = 0 \ ; \\ \partial_t(\epsilon m_k U_k) + \partial_x\left(\epsilon m_k U_k^2\right) + \epsilon \alpha_k \partial_x(P_k) + \epsilon(P_k - P_I)\partial_x(\alpha_k) = \epsilon D_k(W) \ ; \\ \partial_t(\epsilon E_k) + \partial_x(\epsilon U_k(E_k + \alpha_k P_k)) + \epsilon P_I \partial_t(\alpha_k) = \epsilon \psi_k + \epsilon V_I D_k(W) \ . \end{array} \right. \tag{3}$$

We now detail the closure laws for the source terms (ϕ_2, D_k, ψ_k), which agree with :

$$\sum_{k=1}^{2} \psi_k(W) = 0 \quad ; \quad \sum_{k=1}^{2} D_k(W) = 0 \quad ; \quad \sum_{k=1}^{2} \phi_k(W) = 0 \ . \tag{4}$$

The latter two read:

$$\left\{ \begin{array}{l} D_k = (-1)^k \frac{m_1 m_2}{(m_1+m_2)}(U_1 - U_2)/\tau_U \ ; \\ \phi_k = (-1)^k \frac{\alpha_1 \alpha_2}{|P_1|+|P_2|}(P_2 - P_1)/\tau_P \ . \end{array} \right. \tag{5}$$

where both τ_U and τ_P denote relaxation time scales. The contribution D_k refers to the drag forces. Besides, the energy interfacial transfer term :

$$\psi_k = K_T(a_k - a_{3-k}) \tag{6}$$

requires to define a_k:

$$a_k = (s_k)^{-1}(\partial_{P_k}(s_k))(\partial_{P_k}(e_k))^{-1} \tag{7}$$

where $s_k = s_k(P_k, \rho_k)$ denotes the specific entropy, which is compelled with:

$$(c_k)^2 \partial_{P_k}(s_k) + \partial_{\rho_k}(s_k) = 0 \tag{8}$$

noting as usual:

$$(c_k)^2 = (c_k)^2(P_k, \rho_k) = \left(\frac{P_k}{(\rho_k)^2} - \partial_{\rho_k}(e_k)\right)(\partial_{P_k}(e_k))^{-1} \tag{9}$$

The couple (V_I, P_I) is assumed to be one among the two couples (U_k, P_{3-k}), with $k \in 1,2$. For instance, the pair (U_2, P_1) is expected to be physically relevant when the phase 2 is dilute (and reversely the pair (U_1, P_2) when the flow is dominated by phase 2). these two pairs correspond to models investigated in[1,3,25,28,29] among others. Note anyway that a third choice corresponding to (V_m, P_m) as defined in[8,13] is also meaningful, and might be considered as well.

B. Main properties of the two-fluid model

First, we focus on the homogeneous part of (3), eg:

$$\begin{cases} \partial_t(\epsilon) = 0 \ ; \\ \partial_t(\alpha_2) + V_I \partial_x(\alpha_2) = 0 \ ; \\ \partial_t(\epsilon m_k) + \partial_x(\epsilon m_k U_k) = 0 \ ; \\ \partial_t(\epsilon m_k U_k) + \partial_x\left(\epsilon m_k U_k^2\right) + \epsilon\alpha_k \partial_x(P_k) + \epsilon(P_k - P_I)\partial_x(\alpha_k) = 0 \ ; \\ \partial_t(\epsilon E_k) + \partial_x(\epsilon U_k(E_k + \alpha_k P_k)) + \epsilon P_I \partial_t(\alpha_k) = 0 \ . \end{cases} \tag{10}$$

Property 1 (Structure of the convective part of (3)):
The homogeneous system (10) *admits the following real eigenvalues:*

$$\begin{array}{lllll} \lambda_0 = 0 & , & \lambda_1 = V_I, & & \\ \lambda_2 = U_1 & , & \lambda_3 = U_1 - c_1 & , & \lambda_4 = U_1 + c_1, \\ \lambda_5 = U_2 & , & \lambda_6 = U_2 - c_2 & , & \lambda_7 = U_2 + c_2 \end{array} \tag{11}$$

Associated right eigenvectors span the whole space if : $|V_I - U_k| \neq c_k$, *and* $|U_k| \neq c_k$, *for* $k = 1, 2$. *Otherwise, a resonance phenomenum occurs. Fields associated with eigenvalues* $\lambda_0, \lambda_2, \lambda_5$ *are linearly degenerated (LD), whereas fields associated with* $\lambda_3, \lambda_4, \lambda_6, \lambda_7$ *are genuinely non-linear. Owing to the particular choice* $V_I = U_k$, *the field associated with* λ_1 *is also LD.*

For nuclear applications with a mixture of water and vapour, resonance is very unlikely to happen, since material velocities are indeed small compared with the speed of acoustic waves in pure phases. For a more detailed investigation of resonance phenomena, we refer for instance to[15] and also to[7] which focuses on shallow-water equations with topography.

Property 2 (Entropy inequality):
Define the entropy-entropy flux pair (η, f_η) *as:*

$$\eta = \epsilon(m_1 Log(s_1) + m_2 Log(s_2))$$

$$f_\eta = \epsilon(m_1 Log(s_1) U_1 + m_2 Log(s_2) U_2)$$

and the following quantity:

$$m_k R_k = a_k(\psi_k + D_k(V_I - U_k) - \phi_k(P_I - P_k)) \tag{12}$$

Then smooth solutions of system (3) *comply with the following entropy inequality :*

$$\partial_t(\eta) + \partial_x(f_\eta) = \epsilon(m_1 R_1 + m_2 R_2) \geq 0 \ . \tag{13}$$

Before going further on, it may be noticed that slightly different choices of P_I might be considered (see [24,8,13]), which result in a dissipative contribution in the governing equation of the entropy η. We insist that these are not considered in the present paper.

Property 3 (Riemann invariants in the standing wave):
The linearly degenerated (LD) wave associated with $\lambda = 0$ *admits the following Riemann invariants*

$$\begin{array}{llll} I_1^0(W) = \alpha_2 & ; & I_2^0(W) = s_1 & ; \quad I_3^0(W) = \epsilon m_1 U_1 \quad ; \\ I_4^0(W) = e_1 + \frac{P_1}{\rho_1} + \frac{U_1^2}{2} & ; & I_5^0(W) = s_2 & ; \\ I_6^0(W) = \epsilon m_2 U_2 & ; & I_7^0(W) = e_2 + \frac{P_2}{\rho_2} + \frac{U_2^2}{2} & \end{array}$$

The latter Riemann invariants will be used in practice in order to define the third scheme in section IV.

Property 4 (Riemann invariants in the V_I contact discontinuity):
We still assume that $V_I = U_k$. As a consequence, the wave associated with the eigenvalue $\lambda = V_I$ is linearly degenerated. Moreover, associated Riemann invariants are the following:

$$\begin{array}{l} I_1^1(W) = \epsilon \quad ; \quad I_2^1(W) = s_{3-k} \quad ; \\ I_3^1(W) = U_k \quad ; \quad I_4^1(W) = m_{3-k}(U_{3-k} - U_k) \quad ; \\ I_5^1(W) = \alpha_1 P_1 + \alpha_2 P_2 + m_{3-k}(U_{3-k} - U_k)^2 \quad ; \\ I_6^1(W) = e_{3-k} + \frac{P_{3-k}}{\rho_{3-k}} + \frac{1}{2}(U_{3-k} - U_k)^2 \end{array}$$

The latter property is obviously extremely important. Actually, even in a free medium, thus corresponding to the uniform distribution $\epsilon = 1$, the specific closure law for the so-called interfacial velocity-pressure pair (V_I, P_I) guarantees that the non-conservative products are only active in a linearly degenerated field. Thus unique jump conditions hold field by field, which results in the crucial point that the converged approximations (w.r.t. the mesh size) obtained when computing flows with shock waves through system (3) will not depend on the scheme (see[21]), as may happen for other unsuitable choices of (V_I, P_I).

III. Basic solutions

A. Two simple solutions

We define two basic solutions of system (3), whatever the EOS is.

- *Basic solution S_1:*
  We define solution S_1 as the following *unsteady* solution:

$$\left\{ \begin{array}{l} \epsilon(x) = \epsilon_0 \\ P_1(x,t) = P_2(x,t) = P_0 \\ U_1(x,t) = U_2(x,t) = U_0 \end{array} \right. \tag{14}$$

  while both ρ_k and α_2 are solutions of the governing equation:

$$\partial_t(f) + U_0 \partial_x(f) = 0$$

  Note that this solution, which is only valid in a free medium, may be viewed as a solution of the sole convective part of system (3), or alternatively of the full set of equations (3).

- *Basic solution S_2:*
  We assume that the distribution $\epsilon(x)$ is arbitrary. Solution S_2 will correspond to the *steady* solution:

$$\left\{ \begin{array}{l} P_1(x,t) = P_2(x,t) = P_0 \\ U_1(x,t) = U_2(x,t) = 0 \end{array} \right. \tag{15}$$

  while both $m_k(x,t) = m_k(x,0)$ and $\alpha_2(x,t) = \alpha_2(x,0)$.

These two basic solutions will be used in order to define *a priori* suitable schemes. The second solution S_2 will also be used as a preliminary test case (test 2) in numerical experiments in section VI.

B. Solutions of the Riemann problem

We focus here the homogeneous part of system (3), and thus consider now solutions of the Riemann problem associated with system (10). *We must insist here that we do not know whether there exists a unique solution to the one dimensional Riemann problem for our problem, given left and right initial states.* However, we may proceed differently and construct exact solutions. For that purpose we simply introduce a left initial condition, and then construct intermediate states and associated single waves, choosing an initial configuration. We shall restrict here to rather simple choices involving "ghost" waves -through which no variation of the state variable occurs-, and: (i) a steady contact discontinuity, and/or (ii) a moving V_I contact discontinuity and/or (iii) a shock wave in phase 2. Solutions will be referred to as Test 1, Test 3 and Test 4 respectively.

Of course much more complex test cases might be defined that way, such as those examined in[1,28,29] for instance, but we emphasize here once more that we want to focus on situations where the porosity varies, which explains our choices. The exact construction of intermediate states and the final right state is detailed in appendix A. Numerical values that are used in numerical experiments are recalled at the beginning of section VI, which is devoted to the measure of the L^1 norm of the error.

The figure below provides a sketch of the solution of Riemann problems that will be investigated, together with notations :

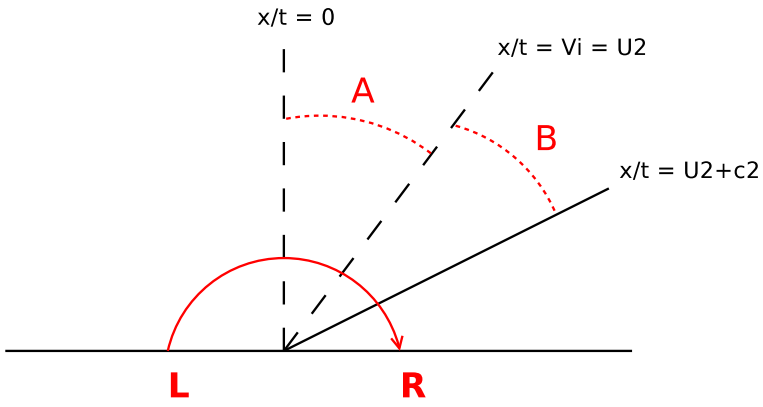

Figure 1. Sketch of the specific fan of waves in exact solutions and notations for intermediate states.

IV. Finite Volume schemes

We introduce standard notations for Finite Volume schemes (see[9]). Within each Finite Volume of size $h_i = x_{i+1/2} - x_{i-1/2}$, the mean value of W at time t^n in cell i is:

$$W_i^n = (\int_{[x_{i-1/2},x_{i+1/2}]} W(x,t^n)dx)/h_i \tag{16}$$

The time step Δt^n will comply with a standard CFL condition. Moreover, we define:

$$\overline{a}_{i+1/2} = (a_i + a_{i+1})/2$$

whatever the quantity a is, and also:

$$(\Delta(\overline{a}))_i^n = (\overline{a})_{i+1/2}^n - (\overline{a})_{i-1/2}^n$$

for $k = 1, 2$.

We define the flux f_ϵ in $\mathbf{R}^6$:

$$f_\epsilon(W_\epsilon, \alpha_2, \epsilon)^t = (\epsilon m_k U_k, \epsilon m_k U_k^2, \epsilon U_k(E_k + \alpha_k P_k)) \tag{17}$$

The computation of the whole set (3) is achieved with a fractional step method which is in agreement with the overall entropy inequality. The homogeneous problem associated with (10) is computed first. Source terms are then accounted for using an implicit scheme, which is exactly the one described in reference[13] . We thus only describe the first evolution step here.

A. Classical Rusanov scheme R

The cell scheme which is used to compute the evolution step simply reads:

$$h_i((\alpha_2)_i^{n+1} - (\alpha_2)_i^n) + \Delta t^n (V_I)_i^n (\Delta(\overline{\alpha}_2))_i^n + \Delta t^n (c_{i+1/2}^n - c_{i-1/2}^n) = 0 \tag{18}$$

where $c^n_{i+1/2} = -r^n_{i+1/2}((\alpha_2)^n_{i+1} - (\alpha_2)^n_i)/2$, while:

$$h_i((W_\epsilon)^{n+1}_i - (W_\epsilon)^n_i) + \Delta t^n(F^R_{i+1/2}((W_\epsilon)^n_l, (\alpha_2)^n_l, \epsilon_l) - F^R_{i-1/2}((W_\epsilon)^n_l, (\alpha_2)^n_l, \epsilon_l)) + \Delta t^n (H_\epsilon)^n_i = 0 \tag{19}$$

where the numerical flux is defined by:

$$F^R_{i+1/2}((W_\epsilon)^n_l, (\alpha_2)^n_l, \epsilon_l) = \Big(f_\epsilon((W_\epsilon)^n_i, (\alpha_2)^n_i, \epsilon_i) + f_\epsilon((W_\epsilon)^n_{i+1}, (\alpha_2)^n_{i+1}, \epsilon_{i+1}) - r^n_{i+1/2}((W_\epsilon)^n_{i+1} - (W_\epsilon)^n_i) \Big)/2 \tag{20}$$

The notation $(W_\epsilon)^n_l$ involves the stencil l that refers to cell indices $(i, i+1)$ for $F_{i+1/2}$, (respectively to $(i-1, i)$ for $F_{i-1/2}$). The scalar $r^n_{i+1/2}$ represents the maximal value of the spectral radius of the Jacobian matrices $A((W_\epsilon)^n_l, (\alpha_2)^n_l, \epsilon_l)$ for $l = i, i+1$. The contribution connected with the first-order non-conservative terms $(H_\epsilon)^n_i$ is approximated by:

$$(H_\epsilon)^n_i = (0, \epsilon_i(((P_k)^n_i - (P_I)^n_i)(\Delta(\overline{\alpha}_k))^n_i + (\alpha_k)^n_i(\Delta(\overline{P}_k))^n_i), -\epsilon_i(P_I)^n_i(V_I)^n_i(\Delta(\overline{\alpha}_k))^n_i) \tag{21}$$

B. A modified Rusanov scheme MR

This scheme is similar to the previous one. Its main interest is that it guarantees that the steady solution S_2 will be perfectly approximated on any mesh size (see section V below).

The update for the void fractions is:

$$h_i((\alpha_2)^{n+1}_i - (\alpha_2)^n_i) + \Delta t^n (V_I)^n_i (\Delta(\overline{\alpha}_2))^n_i + \Delta t^n (d^n_{i+1/2,-} - d^n_{i-1/2,+}) = 0 \tag{22}$$

where :

$$\begin{aligned} d^n_{i+1/2,-} &= -(\hat{\epsilon})_{i+1/2} r^n_{i+1/2}((\alpha_2)^n_{i+1} - (\alpha_2)^n_i)/(2\epsilon_i) \\ d^n_{i-1/2,+} &= -(\hat{\epsilon})_{i-1/2} r^n_{i-1/2}((\alpha_2)^n_i - (\alpha_2)^n_{i-1})/(2\epsilon_i) \end{aligned} \tag{23}$$

The numerical flux in (19) is replaced by:

$$F^{MR}_{i+1/2}((W_\epsilon)^n_l, (\alpha_2)^n_l, \epsilon_l) = \Big(f_\epsilon((W_\epsilon)^n_i, (\alpha_2)^n_i, \epsilon_i) + f_\epsilon((W_\epsilon)^n_{i+1}, (\alpha_2)^n_{i+1}, \epsilon_{i+1}) - r^n_{i+1/2}(\hat{\epsilon})_{i+1/2}(\tfrac{(W_\epsilon)^n_{i+1}}{\epsilon_{i+1}} - \tfrac{(W_\epsilon)^n_i}{\epsilon_i}) \Big)/2 \tag{24}$$

where $(\hat{\epsilon})_{i+1/2} = max(\epsilon_i, \epsilon_{i+1})$, or : $(\hat{\epsilon})_{i+1/2} = (2\epsilon_i\epsilon_{i+1})/(\epsilon_i + \epsilon_{i+1})$.

C. A simplified well-balanced scheme WBR

The basic idea is the following. For the sake of simplicity, we introduce $Z \in \mathbf{R}^7$ and $f(Z) \in \mathbf{R}^7$ as follows:

$$\begin{aligned} Z^t &= (\alpha_2, m_k, m_k U_k, E_k) \\ f(Z)^t &= (0, m_k U_k, m_k U_k^2 + \alpha_k P_k, U_k(E_k + \alpha_k P_k)) \end{aligned} \tag{25}$$

Now, since ϵ is assumed to be constant within each cell, the cell scheme will read:

$$h_i(Z^{n+1}_i - Z^n_i) + \Delta t^n (F^{WBR}_{i+1/2,-}(Z^n_l, \epsilon_l) - F^{WBR}_{i-1/2,+}(Z^n_l, \epsilon_l)) + \Delta t^n H^n_i = 0 \tag{26}$$

where the numerical fluxes and the contribution H are defined by:

$$\begin{aligned} F^{WBR}_{i+1/2,-}(Z^n_l, \epsilon_l) &= \Big(f(Z^n_i) + f(Z^n_{i+1/2,-}) - (r_{WB})^n_{i+1/2}(Z^n_{i+1/2,-} - Z^n_i) \Big)/2 \\ F^{WBR}_{i-1/2,+}(Z^n_l, \epsilon_l) &= \Big(f(Z^n_i) + f(Z^n_{i-1/2,+}) - (r_{WB})^n_{i-1/2}(Z^n_i - Z^n_{i-1/2,+}) \Big)/2 \end{aligned} \tag{27}$$

$$H^n_i = ((V_I)^n_i(\Delta(\overline{\alpha}_2))^n_i, 0, -(P_I)^n_i(\Delta(\overline{\alpha}_k))^n_i, -(P_I)^n_i(V_I)^n_i(\Delta(\overline{\alpha}_k))^n_i) \tag{28}$$

The values $Z^n_{i-1/2,+}$ and $Z^n_{i+1/2,-}$ are obtained by solving the non-linear equations (for $m = 0$ to 6):

$$\begin{aligned} Inv^0_m(Z^n_{i-1/2,+}, \epsilon_i) &= Inv^0_m(Z^n_{i-1}, \epsilon_{i-1}) \\ Inv^0_m(Z^n_{i+1/2,-}, \epsilon_i) &= Inv^0_m(Z^n_{i+1}, \epsilon_{i+1}) \end{aligned} \tag{29}$$

In agreement with section II (property 3), we have set here:

$$\begin{array}{l} Inv_0^0(Z,\epsilon) = \alpha_2 \\ Inv_{3k-2}^0(Z,\epsilon) = s_k \\ Inv_{3k-1}^0(Z,\epsilon) = \epsilon m_k U_k \\ Inv_{3k}^0(Z,\epsilon) = e_k + P_k/\rho_k + U_k^2/2 \end{array} \tag{30}$$

for $k = 1, 2$. In practice, this requires solving two uncoupled non-linear scalar equations (one for each phase) at each cell interface $i + 1/2$, the solution of which is trivial when $\epsilon_i = \epsilon_{i+1}$, or when $(U_k)_i^n (U_k)_{i+1}^n = 0$. Details pertaining to the exact solution of the above-mentionned equations are given in appendix C. We emphasize here that:

$$max(|(U_k)_{i+1/2,-}^n|, |(U_k)_{i+1/2,+}^n|, r_l^n) = (r_{WB})_{i+1/2}^n \qquad \text{for} \quad k = 1, 2$$

where r_l^n stands for the spectral radius of the Jacobian matrix at time t^n for $l = i, i + 1$.

We note that the update for α_2 is exactly the same as the one achieved in (18), owing to the specific value of $Inv_0^0(Z,\epsilon)$ (which implies that : $(\alpha_2)_{i+1/2,-}^n = (\alpha_2)_{i+1}^n$ and $(\alpha_2)_{i-1/2,+}^n = (\alpha_2)_{i-1}^n$). Obviously when the porosity is uniform ($\epsilon_{i-1} = \epsilon_i = \epsilon_{i+1}$), this scheme identifies with the standard Rusanov scheme, since $Z_{i-1/2,+}^n = Z_{i-1}^n$ and $Z_{i+1/2,-}^n = Z_{i+1}^n$ in that case, and it also corresponds to scheme MR.

V. Main properties

We wonder first whether the latter three schemes preserve basic solutions on any mesh, which is of course crucial for industrial applications. For that purpose, we need to introduce some constants $a_{k,0}$ for both phases, together with two invertible functions $g_k(\phi)$. Actually, one may easily check that:

- Property 5: *We assume that the EOS takes the form: $\rho_k e_k(P_k, \rho_k) = a_{k,0}\rho_k + g_k(P_k)$ in each phase k. The three schemes R, MR and WBR described above preserve the discrete form of the basic solution S_1, whatever the mesh size is, since $(U_1)_i^n = (U_2)_i^n = U_0$ and $(P_1)_i^n = (P_2)_i^n = P_0$ imply that $(U_1)_i^{n+1} = (U_2)_i^{n+1} = U_0$ and $(P_1)_i^{n+1} = (P_2)_i^{n+1} = P_0$, if $\epsilon_i = \epsilon_0$.*

  The reader is referred to appendix B, section A for proof, which is almost obvious. In practice, standard EOS such as perfect gas EOS or stiffened gas EOS belong to the above mentionned class. We recall that the stiffened gas EOS simply stands for $a_{k,0} = 0$ and $g_k(\phi) = (\phi + \gamma_k \Pi_k)/(\gamma_k - 1)$, where constants γ_k and Π_k are assumed to be such that: $\gamma_k > 1$ and $0 \leq \Pi_k$.

  Of course (see[10] for such a discussion in the framework of homogeneous models), it does not mean *a priori* that the schemes will - or won't- converge towards correct solutions.

  The next property is also useful for practical applications, though it is not sufficient of course. It requires similar assumptions on the form of the EOS.

- Property 6: *We assume that the EOS takes the form: $\rho_k e_k(P_k, \rho_k) = a_{k,0}\rho_k + g_k(P_k)$ in each phase k. Both schemes MR and WBR preserve the discrete form of the basic solution S_2 on any mesh, since $(U_1)_i^n = (U_2)_i^n = 0$ and $(P_1)_i^n = (P_2)_i^n = P_0$ imply that $(U_1)_i^{n+1} = (U_2)_i^{n+1} = 0$ and also $(P_1)_i^{n+1} = (P_2)_i^{n+1} = P_0$, with arbitrary ϵ_i. The standard R scheme does not.*

  A proof is detailed in appendix B, section B, which is again almost obvious, and only requires a few calculations. The structure of the scheme MR with respect to the void fraction is of course mandatory to ensure the result.

- Property 7: *We use notations introduced in section II pertaining to Riemann invariants. If we assume that $\epsilon_L \neq \epsilon_R$, and also that the initial conditions (W_L, W_R) of the Riemann problem comply with :*

$I_m^0(W_L) = I_m^0(W_R)$, for $m = 1$ to 7, we are ensured that the scheme WBR preserves steady states on any mesh. This does not hold true for schemes R and MR.

The proof for schemes R and MR is not detailed here since it is obvious. The one pertaining to scheme WBR is given in appendix B, section C. Actually, it is also close to some results stated in[4] . The proof is also almost the same as the one given in [26] in the case of Euler equations with perfect gas EOS, in a one-dimensional framework, where authors examine the particular case of flows in variable cross section ducts. It occurs in fact in the proof that, though the present system is indeed much more complex than the one examined in [26] , both phases almost "decouple" through the interface, since the void fraction is one among the seven Riemann invariants of the standing wave associated with λ_0 (see section II). A straightforward consequence is that the governing equations for the mass, momentum and total energy within phase k in a porous medium almost behave "locally" as the Euler equations in a porous medium.

- Property 8: *The maximum principle for the void fractions holds, and positive cell values of partial masses are ensured when applying any scheme among R, MR and WBR, provided that the following CFL conditions hold:*

R scheme:

$$\frac{\Delta t^n}{2h_i}(r^n_{i+1/2} + r^n_{i-1/2}) \leq 1 \qquad \forall i \tag{31}$$

MR scheme (with $(\hat{\epsilon})_{i+1/2} = max(\epsilon_i, \epsilon_{i+1})$):

$$\frac{\Delta t^n}{2h_i}\left(\frac{(\hat{\epsilon})_{i+1/2}}{\epsilon_i} r^n_{i+1/2} + \frac{(\hat{\epsilon})_{i-1/2}}{\epsilon_i} r^n_{i-1/2}\right) \leq 1 \qquad \forall i \tag{32}$$

WBR scheme:

$$\frac{\Delta t^n}{2h_i}((r_{WB})^n_{i+1/2} + (r_{WB})^n_{i-1/2}) \leq 1 \qquad \forall i \tag{33}$$

Proofs are given in appendix B, section D.

These results were expected, owing to the specific structure of the underlying Rusanov scheme. The CFL-like condition is almost classical for both R and WBR schemes, and it is slightly different for the MR scheme.

VI. Convergence rate for analytic solutions

We examine in this section the true convergence rate of the above mentionned schemes, when computing Riemann problems as explained in section III. We do not present all results for the three schemes in any case, but we concentrate on the main features, drawbacks and advantages of schemes.

For all cases, we use uniform meshes, and the range of the mesh size will be recalled in each case. The coarser mesh contains 100 cells, whereas the finer mesh contains 8.10^5 cells. More precisely, we use:

Schemes	R	MR	WBR
Test case 1	10^2 to 2.10^5 cells		
Test case 2	10^2 to 2.10^5 cells	10^2 to 2.10^5 cells	10^2 to 2.10^5 cells
Test case 3	10^2 to 4.10^5 cells	-	-
Test case 4	10^2 to 4.10^5 cells	10^2 to 4.10^5 cells	10^2 to 8.10^5 cells

The EOS for the vapour phase ($k = 2$) and the water phase ($k = 1$) are assumed to be perfect gas EOS, and the corresponding constants will be $\gamma_1 = 1.1$ and $\gamma_2 = 1.4$.

The measure of the L^1 norm of the error will be provided, together with a "local" estimation of the convergence rate when meaningful. To be more complete, we recall that we use the pair $(V_I, P_I) = (U_2, P_1)$. In all computations, we use a CFL number 1/2 in order to compute the value Δt^n at each time step. We also recall below the main configurations that will be investigated, as explained in section III.

TEST 1 : Free medium

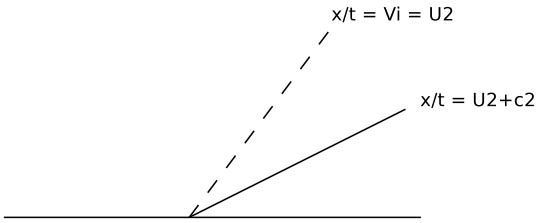

TEST 2 : Solution S_2

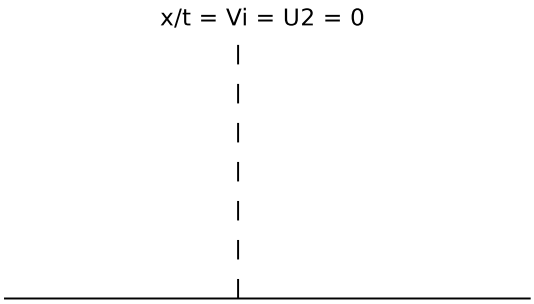

TEST 3 : double contact discontinuity

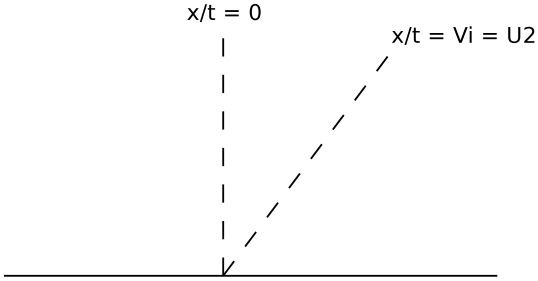

TEST 4 : three-wave pattern

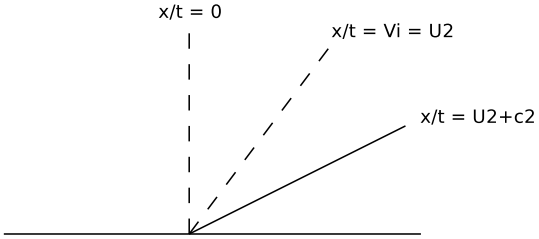

A. Test case 1: A two-wave Riemann problem in a free medium

The first solution corresponds to a very simple flow pattern in a free medium. It only involves one void fraction contact-discontinuity (associated with $\lambda = U_2$), and a shock wave in the vapour phase corresponding to the eigenvalue $\lambda_7 = U_2 + c_2$. Thus left and right initial states are separated by an intermediate state labelled B. We provide below the exact initial data. We recall that results obtained with R, MR, WBR schemes are identical for this test case in a free medium.

	state L	state B	state R
ϵ	1		
α_1	0.95	0.05	
ρ_1	1	0.956131034	
U_1	10	-84.3587663	
P_1	100000	95185.1407	
ρ_2	0.1	0.15	0.1
U_2	15		-357.299567
P_2	10000	95044.7777	53462.6875

Computations have been performed using regular meshes with 10^2, 5.10^2, 10^3, 5.10^3, 10^4, 5.10^4, 10^5, and 2.10^5 cells. These enable to plot the L^1 norm of the error e_h -in logarithmic coordinates- in Figure 2.

One may deduce the measure of the rate of convergence β at time $t = T$, while focusing on the four finer meshes, and enforcing the behaviour $e_h^\phi(T) = C_\phi(T) h^{\beta(\phi)}$.

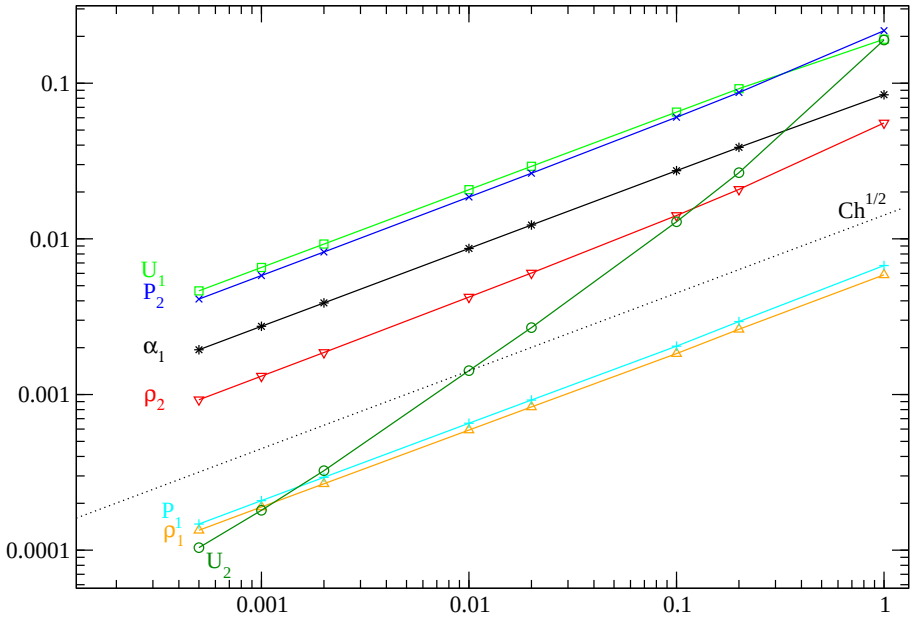

Figure 2. L_1 **norm of the error for the** R **scheme when computing test case 1 (flow in a free medium) as a function of the mesh size.**

	between 10^4 and 5.10^4 cells	between 5.10^4 and 10^5 cells	between 10^5 and 2.10^5 cells
α_1	0.500	0.500	0.500
ρ_1	0.494	0.496	0.497
U_1	0.499	0.500	0.500
P_1	0.497	0.498	0.498
ρ_2	0.509	0.505	0.503
U_2	0.919	0.846	0.797
P_2	0.505	0.503	0.502

These values of $\beta(\phi)$ were actually expected. When restricting to ρ_1, U_1, P_1, and on α_1 which only vary in this test case through the void fraction contact discontinuity, an asymptotic rate of 0.5 is "perfect". Moreover, since (ρ_2, P_2) vary through both waves, the same is expected. *A contrario*, the rate $\beta(U_2)$ should be close to 1 since U_2 is a Riemann invariant through the void fraction contact discontinuity. As a matter of fact, the measured value seems to be close to 0.8, and this agrees with measurements performed in[11] .

B. Solution S_2: a simple steady flow with a free/porous interface

We now focus on the behaviour of schemes R, MR and WBR when computing approximations of solution labelled S_2, whose initial data is given below:

	state L	state R
ϵ	1	0.6
α_1	0.95	0.05
ρ_1	1	
U_1	0	
P_1	100000	
ρ_2	2	0.15
U_2	0	
P_2	100000	

Results with R scheme

Simulations involve meshes with 10^2, 5.10^2, 10^3, 5.10^3, 10^4, 5.10^4, 10^5, and 2.10^5 regular cells. Figure 3 displays the L^1 norm of the error e_h.

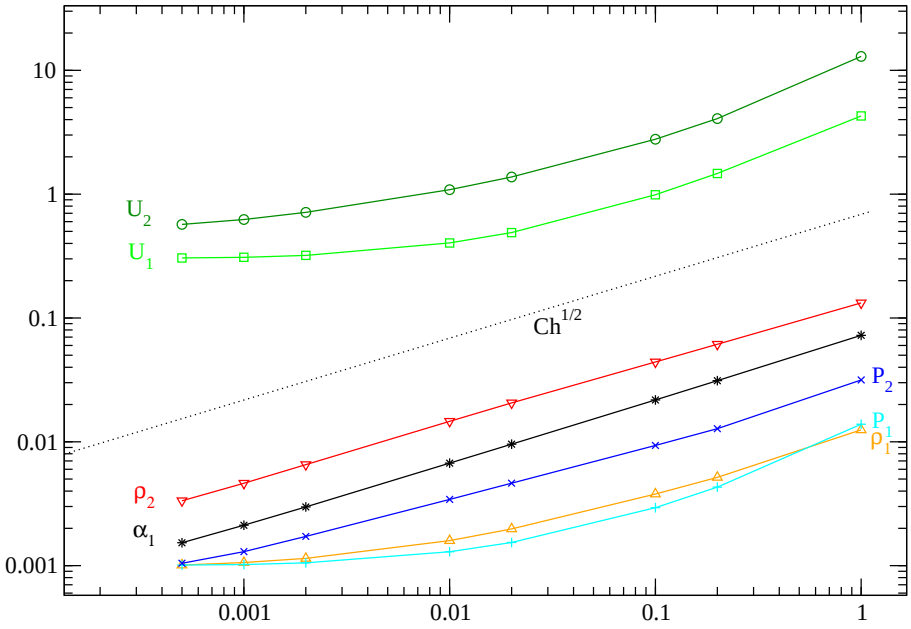

Figure 3. Test 2: L_1 norm of the error for scheme R.

The R scheme clearly no longer converges towards the correct solution when the mesh size goes to zero. The illusion that α_1 and ρ_2 still converge is due to the fact that their initial condition is discontinuous, which dissimulates the uncorrect behaviour on these "coarse" meshes (wrt to what is seeked !). This renders the whole rather dangerous: if we restrict to a range of meshes with 100 up to 10000 cells (the latter represents a "fine mesh" for practical applications...), the R scheme looks almost correct, and one may expect that the pollution will reduce when h tends towards 0...which is obviously not true. Actually, estimations of "convergence rates" $\beta(\phi)$ on the finer meshes are 0.067, 0.017, 0.014 for ρ_1, U_1 and P_1 respectively.

Results with MR scheme

The meshes are exactly the same. The L^1 norm of the error e_h has been plotted in figure 4. Restricting to the finer meshes, approximations of convergence rates $\beta(\phi)$ for ρ_2 and α_1 are clearly 1/2. Round-off errors are observed for all other variables. .

Results with WBR scheme

Meshes are still the same, and results are very similar to those obtained with the latter scheme MR. The L^1 norm of the error e_h has been plotted in figure 5. We have also plotted in figures 6 approximations of both densities ρ_1, ρ_2 that have been obtained using R, MR, WBR schemes on a rather coarse mesh with 1000 nodes. This clearly shows the poor accuracy of the Rusanov scheme: the approximations are spurious around the steady interface, and fast waves propagate on both sides apart from the coupling interface $x = 0.5$. This is of course even more astonishing when looking at the density profile in phase 1.

C. Test 3: a combination of a standing contact wave and a void fraction contact discontinuity

This test case is similar to the second one, but it also involves a contact discontinuity associated with the void fraction wave ($\lambda_5 = U_2$). The intermediate state A has been calculated using appendix A. Meshes now range from 10^2 cells up to 4.10^5 cells. The initial data is as follows:

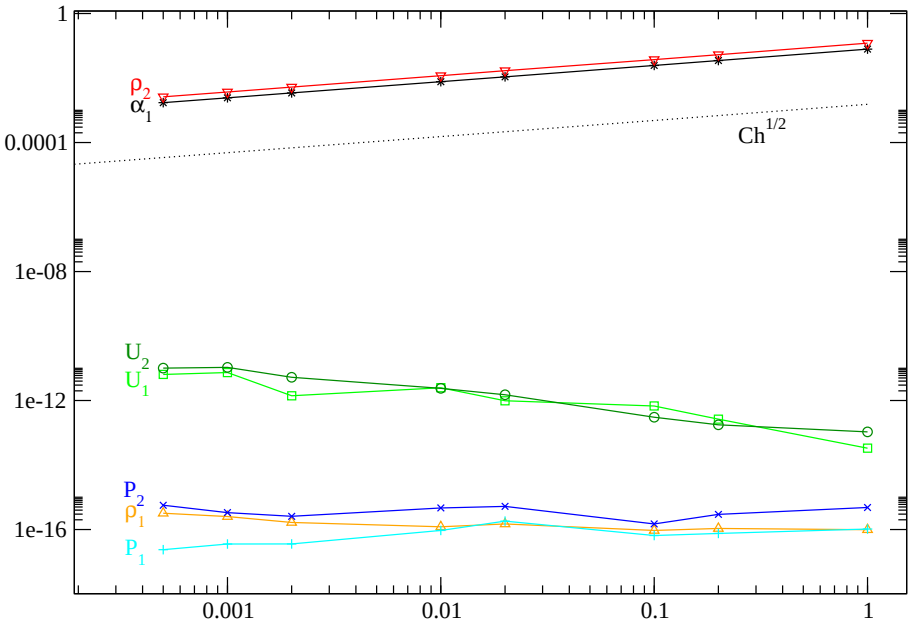

Figure 4. Test 2: L_1 norm of the error for scheme MR.

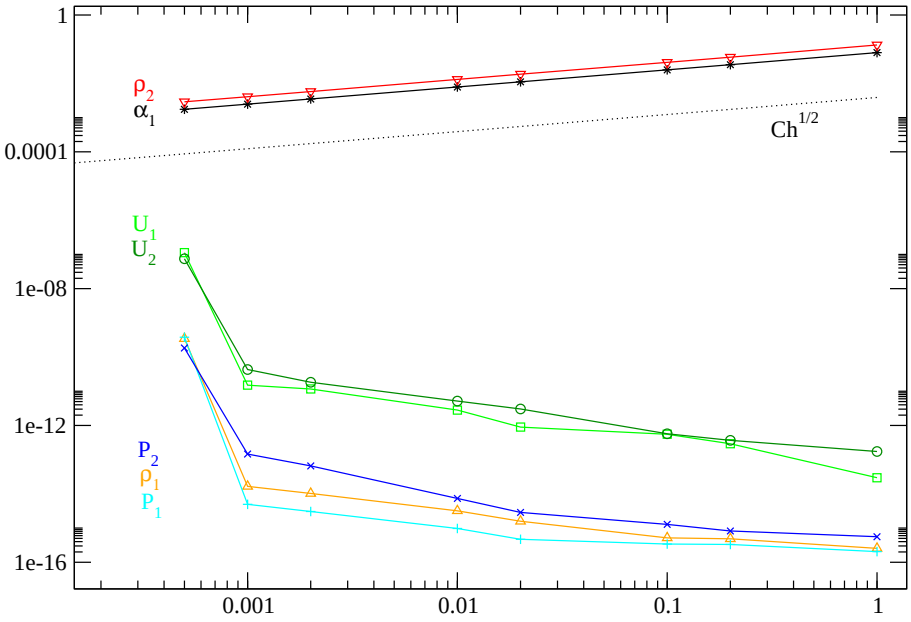

Figure 5. Test 2: L_1 norm of the error for scheme WBR.

	state L	state A	state R
ϵ	1	0.6	
α_1	0.95		0.05
ρ_1	1	0.999190167	0.853058301
U_1	10	16.6801748	−160.919041
P_1	100000	99910.922	83960.8032
ρ_2	0.1	0.0998565629	0.15
U_2	15	25.0359108	
P_2	10000	9979.92457	94534.4211

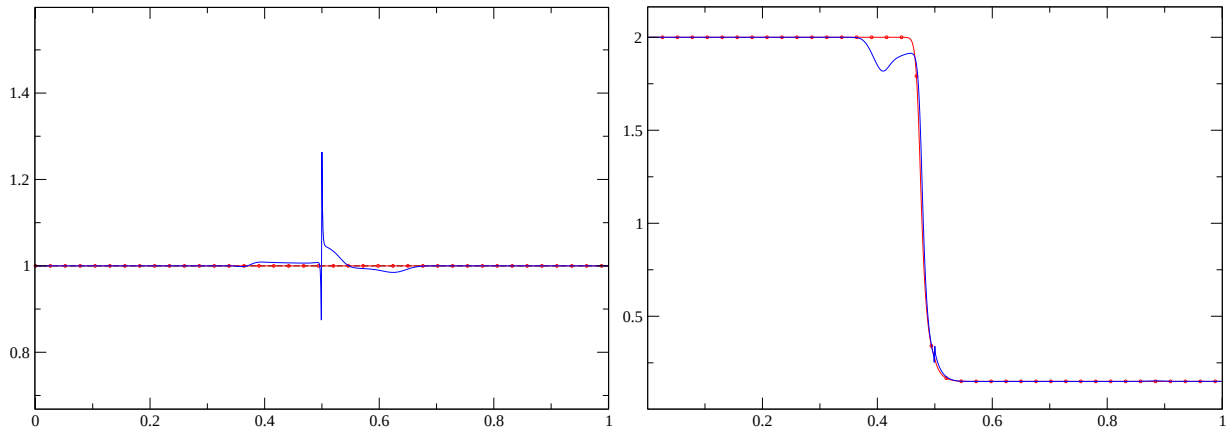

Figure 6. Test 2: density profiles ρ_1, ρ_2 when using schemes R -blue line-, MR -red line with circles-, WBR -black dotted line- on a 1000-cell mesh.

The L^1 norm of the error is plotted in figure 7 when focusing on scheme R.

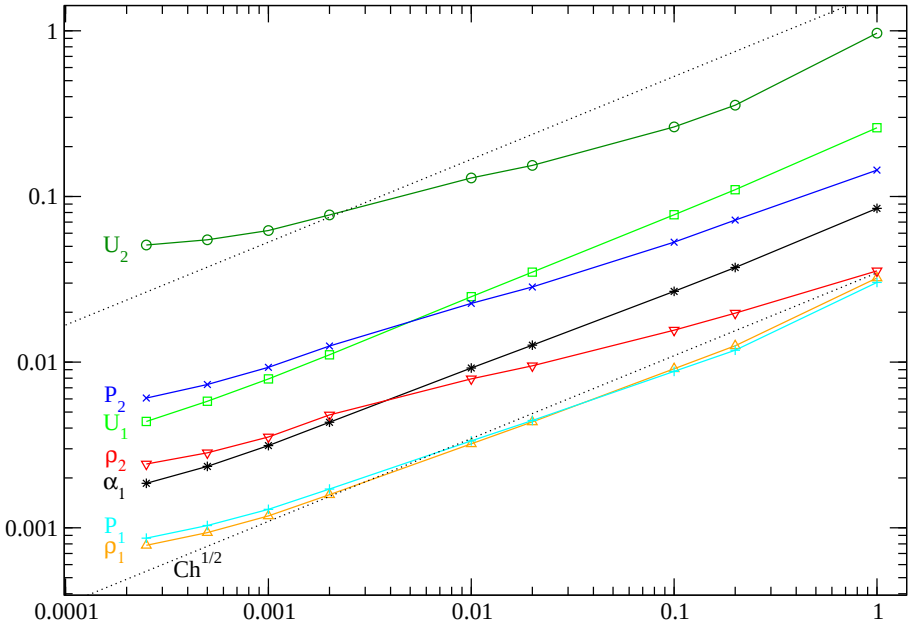

Figure 7. Test 3: L_1 norm of the error for scheme R.

Once again, we may check that the R scheme no longer converges towards the correct solution, which is of course in agreement with the results of test case 2. We emphasize again that the behaviour on the coarser meshes (on the right side in figure 7) is somewhat misleading.

D. Test4: a three-wave pattern

This solution contains two contact waves associated with $\lambda_0 = 0$ and $\lambda_1 = \lambda_5 = U_2$, and one shock wave in the vapour phase corresponding to $\lambda_7 = U_2 + c_2$. The exact initial data is given below:

	state L	state A	state B	state R
ϵ	1	0.6		
α_1	0.95		0.05	
ρ_1	1	0.999190167	0.853058301	
U_1	10	16.6801748	-160.919041	
P_1	100000	99910.922	83960.8032	
ρ_2	0.1	0.0998565629	0.15	0.1
U_2	15	25.0359108		-346.262753
P_2	10000	9979.92457	94534.4211	53175.6119

Still using meshes with 10^2, 5.10^2, 10^3, 5.10^3, 10^4, 5.10^4, 10^5, 2.10^5 and 4.10^5 cells, we check first that the standard Rusanov scheme does not converge towards the correct solution, and then turn to the MR scheme.

Results with MR scheme

First we provide in figure 8 results obtained for $\alpha_2\rho_2$ when computing the test case on a regular mesh with one thousand cells, together with the exact solution. We still consider meshes used in preceeding tests, and errors computed for the MR scheme are given in Figure 9 -on the left side-. The crucial point that occurs is that estimations of convergence rates show evidence that the MR scheme no longer converges towards the correct solution. This is quite obvious when focusing on the U_2 profile in Figure 9. An approximation of the convergence rate for U_2 on the finer meshes is 0.035. It obviously means that the "static" property 6 is far from being sufficient to guarantee convergence of approximations towards the correct solution.

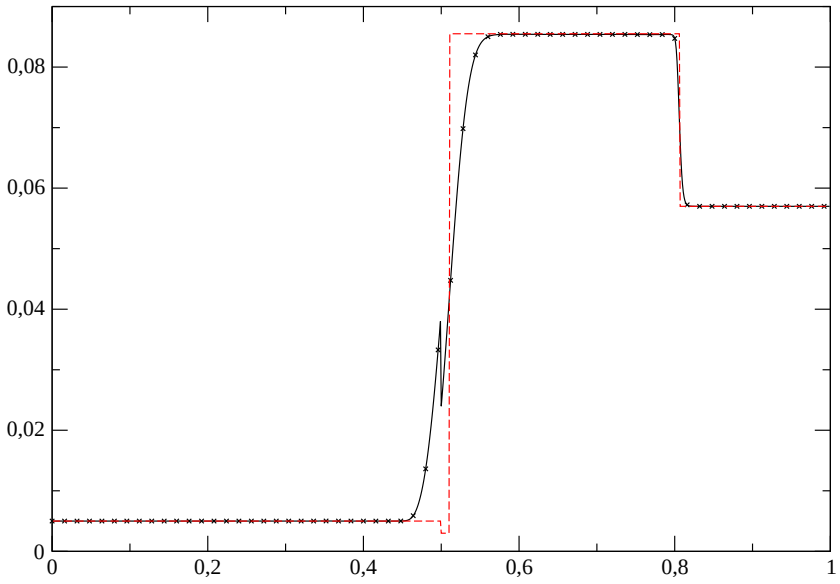

Figure 8. Test 4: mass fraction $\alpha_2\rho_2$ when using MR scheme -black line with crosses- on a 1000-cell mesh, together with the exact solution - red dashed line-.

Results with WBR scheme

Using exactly the same meshes and a finer mesh with 8.10^5 cells, it occurs in Figure 9 (on the right side)that convergence towards the correct solution is now recovered with WBR. Moreover, we retrieve expected rates of convergence $\beta(\phi)$ that are close to 1/2, since all components ϕ vary through at least one contact discontinuity in this fourth test case.

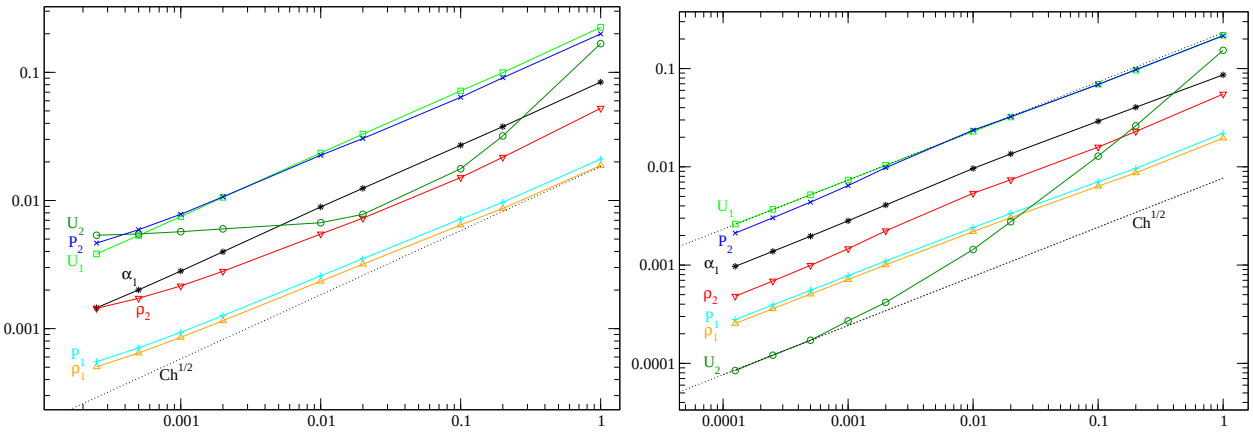

Figure 9. Test 4: L_1 norm of the error for scheme MR (left) and WBR (right) schemes.

	5.10^4 to 10^5 cells	10^5 to 2.10^5 cells	2.10^5 to 4.10^5 cells	4.10^5 to 8.10^5 cells
α_1	0.535	0.521	0.512	0.506
ρ_1	0.495	0.493	0.495	0.496
U_1	0.499	0.495	0.497	0.497
P_1	0.496	0.494	0.496	0.496
ρ_2	0.607	0.562	0.529	0.516
U_2	0.625	0.655	0.505	0.521
P_2	0.607	0.560	0.529	0.516

Local behaviour around the steady interface

We show in figure 10 the behaviour of the discharge $\epsilon m_1 U_1$ around the steady interface $x = 0.5$ when computing the Riemann problem discussed above with MR and WBR schemes, while restricting to a coarse and a rather fine mesh. The WBR scheme provides a reasonable local behaviour around the steady interface, and the amplitude of the reflected wave is indeed much smaller than the one occuring with the MR scheme. Similar remarks hold for $\epsilon m_2 U_2$ and other 0-Riemann invariants.

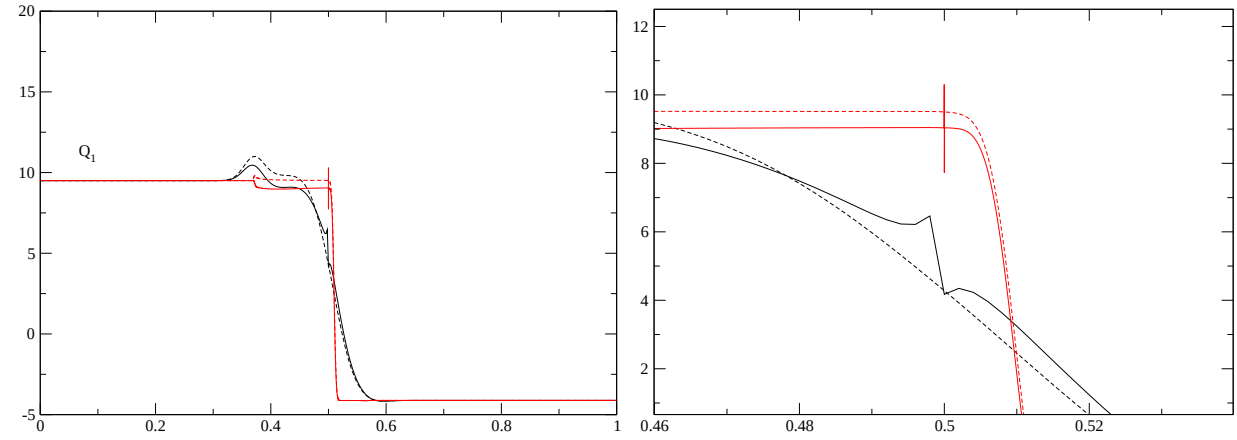

Figure 10. Mean momentum $\epsilon m_1 U_1$ obtained with MR and WBR -dotted line- schemes. The coarse and fine meshes respectively contain 500 -in black- and 50000 -in red- cells. A zoom on $[0.46, 0.54]$ on the right figure provides some more details.

VII. Interaction of fluid waves with the steady interface

We now examine two tests where waves issuing from the free medium propagate towards the porous interface and interact with it. Though we have no analytic solution available in that case, it represents some relevant pattern for industrial applications. The validation of approximations provided by schemes will be evaluated by focusing on the Riemann invariants of the steady wave *computed within each cell*, when the flow is almost steady around the interface. Once again, the CFL number is equal to 1/2 in all cases.

Fifth test case

This test case corresponds to a rough representation of a loss of coolant accident, where we focus on the propagation of the rarefaction wave that will hit a free/porous interface separating the pipe from the steam generator. The computational domain includes a free region ($\epsilon(x < 0.35) = 1$) on the left side of an interface located at $x = 0.35$, and a porous region ($\epsilon(x > 0.35) = 0.6$) on the right side of the latter interface. The whole computational domain thus corresponds to $x \in [0; 1]$. The pipe is suddenly broken around $x = 0.30$, at the beginning of the computation ($t = 0$). Denoting by L, R the left and right states on both sides of the interface $x = 0.30$, the initial conditions are:

	Left state L	Right state R
ϵ	1	0.6
α_1	0.95	0.05
ρ_1	1	
U_1	0	
P_1	1.10^5	1.10^6
ρ_2	20	
U_2	0	
P_2	1.10^5	1.10^6

Figures 11 and 12 show the behaviour of the Riemann invariants H_1, H_2, s_1 and s_2, when the rarefaction has passed the free/porous interface. The mesh contains 1000 regular cells. Subscript 2 now refers to the water phase. The best results are once again obtained with the WBR scheme. Those pertaining to the MR scheme are less spurious than those corresponding to the Rusanov scheme, but show again a non-monotone behaviour.

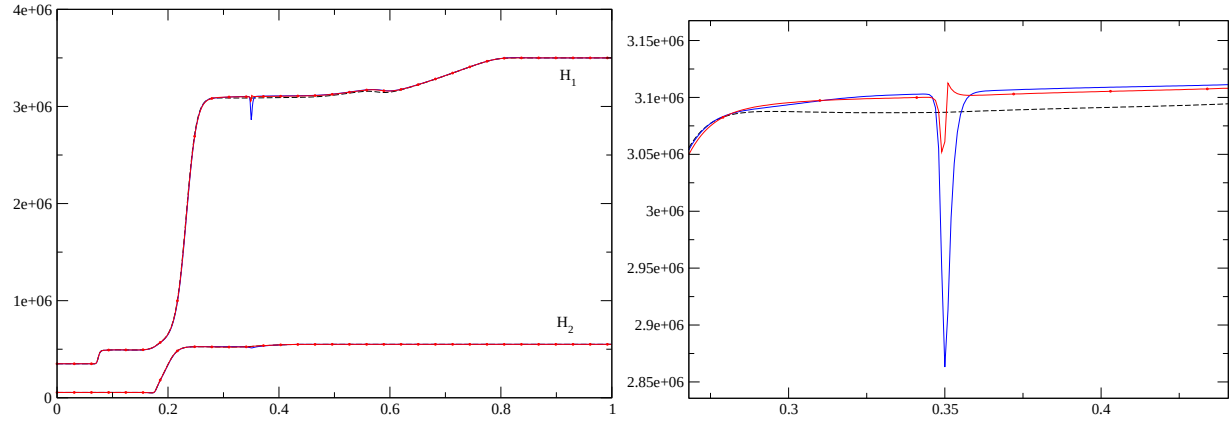

Figure 11. Test case 5: Riemann invariants H_1 and H_2, using a mesh with 1000 cells. The blue line, the red line with circles and the dotted black line correspond to R, MR and WBR schemes respectively. A zoom around the steady interface is displayed on the right for H_1.

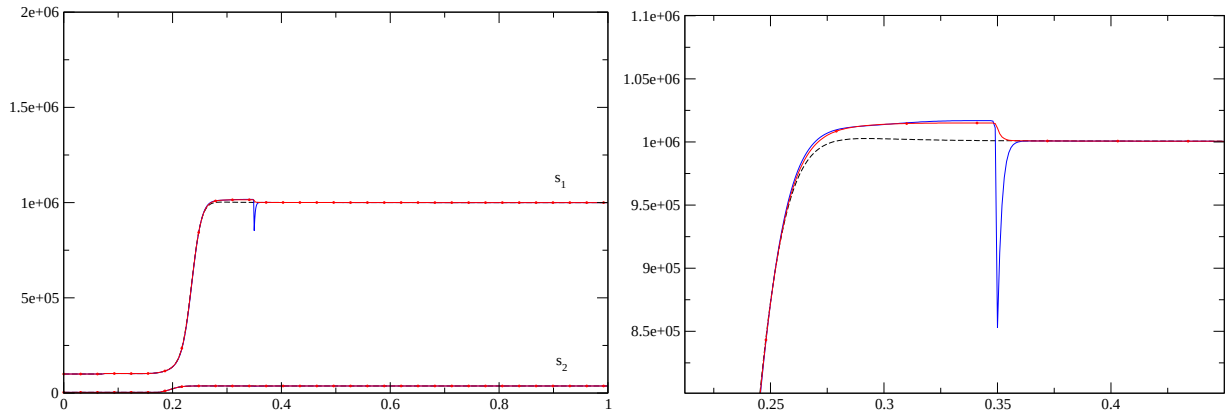

Figure 12. Test case 5: Riemann invariants s_1 and s_2 , using a mesh with 1000 cells. The blue line, the red line with circles and the dotted black line correspond to R, MR and WBR schemes respectively. A zoom around the steady interface is displayed on the right for s_1.

Sixth test case

The initial conditions for this last test case are given in the table below. The computational domain corresponds to $x \in [0; 1]$. The interface between codes is situated at $x = 0.67$, and the porous medium is still on the right side of this interface. Both phases are at rest at the beginning of the computation, and L, R states denote the initial states on the left and right side of $x = 0.65$ respectively. Results for H_1, H_2, s_1 and s_2 are displayed in figures 13 and 14. These have been plotted after the right-going shock waves and the right-going void fraction contact discontinuity have passed the coupling interface ($x = 0.67$).

	Left state L	Right state R
ϵ	1	0.6
α_1	0.05	0.95
ρ_1	1	
U_1	0	
P_1	1.10^6	1.10^5
ρ_2	20	
U_2	0	
P_2	1.10^6	1.10^5

This last test case confirms that the behaviour of WBR scheme is indeed fair.

VIII. Conclusion

- None among the first two schemes R and MR converges towards the correct solution when refining the mesh, if one computes approximations of solutions in very simple one-dimensional Riemann problems involving distinct values of porosity, such as those introduced in section III. Actually, the continuity that is enforced by the Rusanov scheme seems to inhibit the correct convergence when focusing on models for porous media. This is not due to the complexity inherent to the two-fluid approach, and the poor behaviour of these schemes in the framework of Euler equations in variable cross section flows has already been pointed out in the literature (see[27] for instance). However, and to the knowledge of authors, it had never been clearly stated that this drawback was not only annoying for coarse meshes, but also when tackling very fine meshes.
- On the contrary, the WBR scheme, which inherits the spirit of well-balanced schemes combined with the inner stability of Rusanov-like fluxes, provides an extremely simple and useful tool for such computations in porous media. The expected rates of convergence are retrieved, focusing on so-called

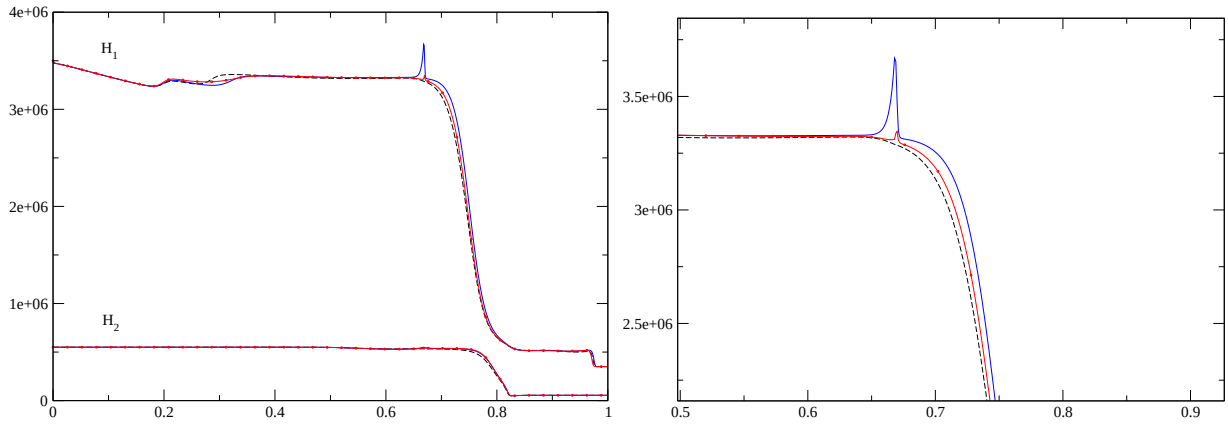

Figure 13. Test case 6: Riemann invariants H_1 and H_2, using a mesh with 1000 cells. The blue line, the red line with circles and the dotted black line correspond to R, MR and WBR schemes respectively. A zoom around the steady interface is displayed on the right for H_1.

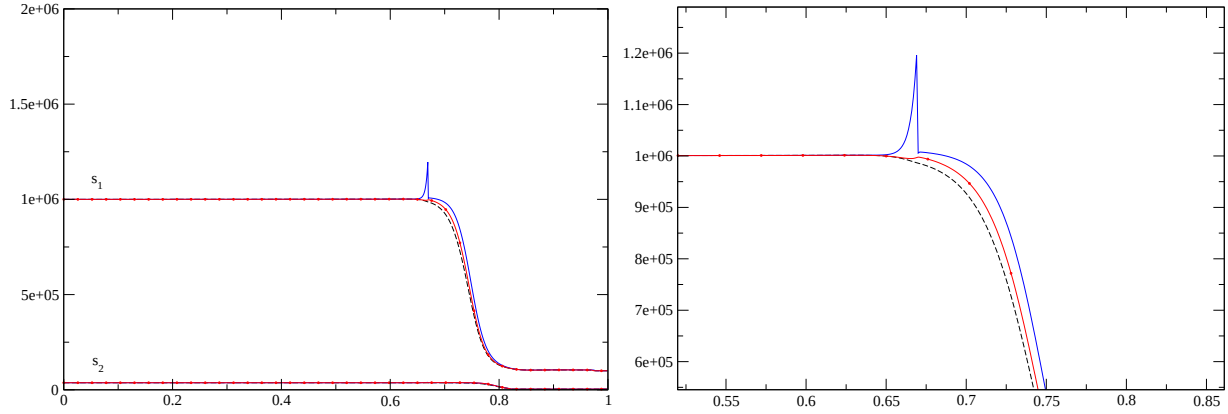

Figure 14. Test case 6: Riemann invariants s_1 and s_2 , using a mesh with 1000 cells. The blue line, the red line with circles and the dotted black line correspond to R, MR and WBR schemes respectively. A zoom around the steady interface is displayed on the right for s_1.

first-order schemes, and the nice behaviour of the discrete cell-values of Riemann invariants of the standing wave around the free/porous interface renders the scheme quite appealing. We recall that this scheme is inspired by the scheme introduced in[27] for Euler equations in variable cross section ducts (see [26] too). It also means that the property 6 is far from being sufficient, and that the dynamical well-balanced property 7 enjoyed by WBR, the continous counterpart of which is property 3, seems mandatory to obtain convergence towards the correct solution.

A straightforward consequence for the NEPTUNE project is that at least one meaningful scheme is available in order to perform the interfacial unsteady coupling of codes that aim at providing approximations of PDEs in free and porous medium respectively.

Among possible improvements and current work in progress in this area, we would like to mention that:

- In order to achieve a better coupling, and more precisely a more relevant treatment of the free/porous interface, we need to provide more physical coupling conditions for momentum equations that might account for the head loss of momentum. This is known to be very tricky, and it is not clear whether direct simulations will *in fine* provide useful tools in practice. A similar remark holds for heat losses through the free/porous interface.

- We also would like to emphasize that an approximate Godunov scheme that inherits a similar well-balanced property may be constructed. This one also makes use of basic ideas introduced by Greenberg and Leroux ([20]), while substituting the approximate Godunov VFRoe-ncv fluxes introduced in[6] to the exact Godunov "fluxes" through the cell interfaces, instead of Rusanov fluxes used in the present work. This of course requires using a suitable variable, as achieved for instance in [22,12] for shallow water equations with topograhy and isentropic Euler equations in a porous medium. The main advantage of the latter solver is that its accuracy is increased when compared with the scheme introduced in[27] . Its extension to the framework of two-phase two-fluid models is currently in progress and seems feasable, and its counterpart for homogeneous flows also seems rather satisfactory ([22]).
- The extension to the framework of three phase flows in a porous medium is also feasable, following [23] for instance.
- The extension of the present WBR scheme to the framework of three-dimensional flows is straightforward (see[14]), and it provides satisfactory results, while preserving the basic positivity results given in property 8.

Acknowledgments

We would like to thank Frédéric Archambeau and Thierry Gallouët who kindly accepted to read the initial version of the manuscript, which helped much. This work has been achieved in the framework of the NEPTUNE project, with financial support from CEA (Commissariat à l'Energie Atomique), EDF, IRSN (Institut de Radioprotection et Sureté Nucléaire) and AREVA-NP. Part of the financial support of the first author is provided by ANRT (Association Nationale de la Recherche Technique, Ministère de la Recherche) through a EDF/CIFRE contract, and also by FSE (Fonds Social Européen). All computational facilities were provided by EDF.

IX. Appendix A : "Construction of solutions of the Riemann problem"

We detail here the construction of the solutions used in the main part of the paper. We start with a given state L, and then successively calculate states A, B and R. We assume here that the EOS for each phase is given by:

$$(\gamma_k - 1)\rho_k e_k = P_k$$

A. Given parameters

We assume that the left state $(\epsilon_L, \alpha_{2_L}, \rho_{1_L}, \rho_{2_L}, P_{1_L}, P_{2_L}, U_{1_L}, U_{2_L})$ is given (with $(U_2)_L > 0$), and we also choose ϵ_R and α_{2_R}, so that : $\epsilon_L \epsilon_R \neq 0$, $\alpha_{2_L}\alpha_{2_R} \neq 0$ and $\alpha_{1_L}\alpha_{1_R} \neq 0$.

B. Construction of the first intermediate state A :

We first obviously get :

$$\epsilon_A = \epsilon_R$$

Since states L and A are separated by the steady LD wave associated with $\lambda_0 = 0$, their connection is thus ensured by Riemann invariants $I_n^0(W)$, $n = 1, 2, ..., 7$.

- Using Riemann invariant $I_1^0(W)$ provides :

  $$\alpha_{2_A} = \alpha_{2_L}$$

  due to the fact that $U_{2_A} > 0$ (see below).
- Riemann invariants $I_3^0(W)$ and $I_6^0(W)$ enable to write :

$$U_{1_A} = \frac{(\epsilon_L)(\rho_{1_L})(U_{1_L})}{(\epsilon_A)(\rho_{1_A})} \quad ; \quad U_{2_A} = \frac{(\epsilon_L)(\rho_{2_L})(U_{2_L})}{(\epsilon_A)(\rho_{2_A})}$$

Moreover, using Riemann invariants $I_2^0(W)$ and $I_5^0(W)$, we can express both pressures P_{1_A} and P_{2_A} in terms of ρ_{1_A} and ρ_{2_A} respectively:

$$P_{1_A} = P_{1_L}\left(\frac{\rho_{1_L}}{\rho_{1_A}}\right)^{-\gamma_1} \quad ; \quad P_{2_A} = P_{2_L}\left(\frac{\rho_{2_L}}{\rho_{2_A}}\right)^{-\gamma_2}$$

Hence, substituting all these expressions in Riemann invariants $I_4^0(W)$ and $I_7^0(W)$, we need to find solutions of $(g_A)_k(X) = 0$ where :

$$(g_A)_k(X) = \frac{\gamma_k}{\gamma_k - 1} s_{k_L}\left(X^{\gamma_k - 1} - \rho_{k_L}^{\gamma_k - 1}\right) + \frac{1}{2}\left(\left(\frac{\epsilon_L}{\epsilon_R}\right)^2\left(\frac{\rho_{k_L}}{X}\right)^2 - 1\right) U_{k_L}^2$$

wrt to ρ_{k_A}.

If $U_{k_L} = 0$, $(g_A)_k(X) = 0$ admits a unique solution: $\rho_{k_A} = \rho_{k_L}$. Otherwise, the function $(g_A)_k(X)$ is decreasing in $]0, X_{min_A,k}]$, and then increasing in $]X_{min_A,k}, +\infty[$, setting :

$$X_{min_A,k} = \left(\frac{U_{k_L}^2\left(\frac{\epsilon_L}{\epsilon_R}\right)^2 (\rho_k)_L^2}{\gamma_k (s_k)_L}\right)^{\frac{1}{\gamma_k + 1}}$$

and we also have $lim(g_A)_k(X) = +\infty$ when X tends to 0 (or $+\infty$). Thus, $(g_A)_k(X) = 0$ may admit two solutions in the general case, no solution if $(g_A)_k(X_{min_A,k}) > 0$).

Once ρ_{k_A} has been calculated, we may use initial expressions to deduce U_{k_A} and P_{k_A}, for $k = 1, 2$.

In practice, for the test cases defined in the main section, we have used the solution ρ_{k_A} that has the same sonic regime than ρ_{k_L}.

C. Construction of the intermediate state B :

States A and B are separated by the contact discontinuity associated with $\lambda_1 = V_I = U_2$. The jump of α_2 is located here, so that : $\alpha_{2_B} = \alpha_{2_R}$.

The remaining components of the intermediate state B are calculated through Riemann invariants $I_n^1(W)$, $n = 1, 2, ..., 6$.

- First of all, by virtue of $I_1^1(W)$, we obviously have $\epsilon_B = \epsilon_A = \epsilon_R$.

  Owing to $I_3^1(W)$, we know that $U_{2_B} = U_{2_A}$. Moreover, $I_4^1(W)$ provides U_{1_B} in terms of ρ_{1_B}:

  $$U_{1_B} = \frac{m_{1_A}}{m_{1_B}}\left(U_{1_A} - U_{2_A}\right) + U_{2_A}$$

  and $I_2^1(W)$ enforces: $P_{1_B} = P_{1_A}\left(\frac{\rho_{1_A}}{\rho_{1_B}}\right)^{-\gamma_1}$

  Eventually, the expression $I_5^1(W)$ enables to calculate P_{2_B} as:

  $$P_{2_B} = \frac{1}{\alpha_{2_R}}\left(\alpha_{1_L} P_{1_A} + \alpha_{2_L} P_{2_A} + m_{1_A} U_{1_A}\left(U_{1_A} - U_{2_A}\right) - \alpha_{1_B} P_{1_B} - m_{1_B} U_{1_B}\left(U_{1_B} - U_{2_B}\right)\right)$$

Hence, substituting all these expressions in the last Riemann invariant $I_6^1(W)$, we conclude that ρ_{1_B} must be a solution of $g_B(X) = 0$ where:

$$g_B(X) = \frac{\gamma_1}{\gamma_1 - 1} s_{1_A} \left(X^{\gamma_1 - 1} - \rho_{1_A}^{\gamma_1 - 1} \right) + \frac{1}{2} \left(\left(\frac{\alpha_{1_L}}{\alpha_{1_R}} \right)^2 \left(\frac{\rho_{1_A}}{X} \right)^2 - 1 \right) (U_{1_A} - U_{2_A})^2$$

- Once again, if $U_{1_A} = U_{2_A}$, there exists only one solution $\rho_{1_B} = \rho_{1_A}$
- Otherwise, we need to solve $g_B(X) = 0$. The procedure is exactly the same as the one discussed in the previous section, where we solve $g_A(X) = 0$ to calculate state A.

- Obviously, owing to the structure of the LD field associated with $\lambda_1 = V_I = U_2$, we need to impose the value of ρ_{2_B}. Thus, state B is completely determined.

D. Construction of the right state R :

We have assumed that states B and R are separated by a GNL wave associated with $\lambda_7 = U_2 + c_2$. We also recall that ϵ_R and α_R have already been set.

This wave is a "ghost" wave for variables in phase 1. Thus:

- $\rho_{1_R} = \rho_{1_B} \quad ; \quad U_{1_R} = U_{1_B} \quad ; \quad P_{1_R} = P_{1_B}$

Turning then to components in phase 2, we face a single-phase problem. Thus we get:

- $\rho_{2_R} = \dfrac{1}{z_R} \rho_{2_B}$ where $z_R \gtrless 1$ must be set, so that $\lambda_7 = U_2 + c_2$ is a shock wave.
- $U_{2_R} = U_{2_B} - c_{2_R} \left(\dfrac{(\beta_2 + 1)(z_R - 1)^2}{\gamma_2 z_R (\beta_2 - z_R)} \right)^{\frac{1}{2}}$ where $\beta_2 = \frac{\gamma_2 + 1}{\gamma_2 - 1}$ and $c_{2_R} = \left(\frac{\gamma_2 P_{2_R}}{\rho_{2_R}} \right)^{\frac{1}{2}}$
- $P_{2_R} = P_{2_B} \dfrac{\beta_2 - z_R}{\beta_2 z_R - 1}$

X. Appendix B : "Main properties of schemes R, MR, WBR"

This appendix is devoted to the proofs of main properties of section V.

A. Property 5

In a free medium, schemes R, MR and WBR are identical. Thus, if $\epsilon_i = \epsilon_0$ for all i, we check it for scheme R. Assume that for given n, $(U_k)_i^n = U_0$ and $(P_k)_i^n = P_0$ for all i $(k = 1, 2)$. We prove now that $(U_1)_i^{n+1} = (U_2)_i^{n+1} = U_0$ and also: $(P_1)_i^{n+1} = (P_2)_i^{n+1} = P_0$, if $\epsilon_i = \epsilon_0$.

The discrete equations that update $(\alpha_k)_i^{n+1}, (m_k)_i^{n+1}, (m_k U_k)_i^{n+1}$ are:

$$\begin{aligned} h_i \left((\alpha_k)_i^{n+1} - (\alpha_k)_i^n \right) \quad & + \Delta t^n U_0 \left((\overline{\alpha_k})_{i+1/2}^n - (\overline{\alpha_k})_{i-1/2}^n \right) \\ & - \tfrac{1}{2} \Delta t^n \left(r_{i+1/2}^n ((\alpha_k)_{i+1}^n - (\alpha_k)_i^n) - r_{i-1/2}^n ((\alpha_k)_i^n - (\alpha_k)_{i-1}^n) \right) = 0 \end{aligned} \tag{34}$$

$$\begin{aligned} h_i \epsilon_0 \left((m_k)_i^{n+1} - (m_k)_i^n \right) \quad & + \Delta t^n \epsilon_0 U_0 \left((\overline{m_k})_{i+1/2}^n - (\overline{m_k})_{i-1/2}^n \right) \\ & - \tfrac{1}{2} \Delta t^n \epsilon_0 \left(r_{i+1/2}^n ((m_k)_{i+1}^n - (m_k)_i^n) - r_{i-1/2}^n ((m_k)_i^n - (m_k)_{i-1}^n) \right) = 0 \end{aligned} \tag{35}$$

$$\begin{aligned} h_i \epsilon_0 \left((m_k U_k)_i^{n+1} - (m_k U_k)_i^n \right) \quad & + \Delta t^n \epsilon_0 (U_0)^2 \left((\overline{m_k})_{i+1/2}^n - (\overline{m_k})_{i-1/2}^n \right) \\ & - \tfrac{1}{2} \Delta t^n \epsilon_0 U_0 \left(r_{i+1/2}^n ((m_k)_{i+1}^n - (m_k)_i^n) - r_{i-1/2}^n ((m_k)_i^n - (m_k)_{i-1}^n) \right) = 0 \end{aligned} \tag{36}$$

Multiplying (35) by U_0, and then substracting the result to the discrete equation of energy in phase k, and using $(U_k)_i^n = U_0$, we obtain:

$$(m_k)_i^{n+1}\left((U_k)_i^{n+1} - U_0\right) = 0$$

which guarantees that for all i:

$$(U_k)_i^{n+1} = U_0 \tag{37}$$

Using now (37), multiplying (36) by a factor $\frac{U_0}{2}$, and substracting the resulting equation to (36) leads to:

$$\begin{array}{ll} h_i\epsilon_0\left((m_ke_k)_i^{n+1} - (m_ke_k)_i^n\right) & +\Delta t^n\epsilon_0 U_0\left((\overline{m_ke_k})_{i+1/2}^n - (\overline{m_ke_k})_{i-1/2}^n\right) \\ & -\frac{1}{2}\Delta t^n\epsilon_0\left(r_{i+1/2}^n((m_ke_k)_{i+1}^n - (m_ke_k)_i^n) - r_{i-1/2}^n((m_ke_k)_i^n - (m_ke_k)_{i-1}^n)\right) = 0 \end{array} \tag{38}$$

We now need to introduce the EOS that takes the form: $\rho_k e_k(P_k,\rho_k) = a_{k,0}\rho_k + g_k(P_k)$ in each phase k. Since $(P_k)_i^n = P_0$ for all i, this implies $(g_k(P_k))_i^n = g_k(P_0)$. Thus, replacing m_ke_k by $a_{k,0}m_k + \alpha_k g_k(P_k)$ in (38), substracting $a_{k,0}$ times (35) and also $\epsilon_0 g_k(P_0)$ times (34) to the discrete equation of energy (38), we get:

$$(\alpha_k)_i^{n+1}\left((g_k(P_k))_i^{n+1} - g_k(P_0)\right) = 0$$

which clearly implies that for all i:

$$(P_k)_i^{n+1} = P_0 \tag{39}$$

This completes the proof of property 5, which means that the three schemes R, MR et WBR preserve the discrete form of solution S_1 on any mesh.

B. Property 6

1. Scheme MR preserves the discrete form of the basic solution S_2 on any mesh

We assume now that $(U_1)_i^n = (U_2)_i^n = 0$ and $(P_1)_i^n = (P_2)_i^n = P_0$. We successively prove that $(U_1)_i^{n+1} = (U_2)_i^{n+1} = 0$ and $(P_1)_i^{n+1} = (P_2)_i^{n+1} = P_0$, whatever ϵ_i is.

Using initial data, the discrete forms of the void fraction/partial mass/momentum take the form:

$$h_i\left((\alpha_k)_i^{n+1} - (\alpha_k)_i^n\right) - \frac{1}{2}\Delta t^n\left(r_{i+1/2}^n\frac{\hat{\epsilon}_{i+1/2}}{\epsilon_i}((\alpha_k)_{i+1}^n - (\alpha_k)_i^n) - r_{i-1/2}^n\frac{\hat{\epsilon}_{i-1/2}}{\epsilon_i}((\alpha_k)_i^n - (\alpha_k)_{i-1}^n)\right) = 0 \tag{40}$$

$$h_i\epsilon_i\left((m_k)_i^{n+1} - (m_k)_i^n\right) - \frac{1}{2}\Delta t^n\left(r_{i+1/2}^n\hat{\epsilon}_{i+1/2}((m_k)_{i+1}^n - (m_k)_i^n) - r_{i-1/2}^n\hat{\epsilon}_{i-1/2}((m_k)_i^n - (m_k)_{i-1}^n)\right) = 0 \tag{41}$$

Owing to the fact that both $(P_k)_i^n = P_0$ and $(U_k)_i^n = 0$, we also get:

$$h_i\epsilon_i\left((m_kU_k)_i^{n+1} - (m_kU_k)_i^n\right) \quad = 0 \tag{42}$$

and thus :

$$(U_k)_i^{n+1} = 0 \tag{43}$$

Still using the EOS such that: $\rho_k e_k(P_k,\rho_k) = a_{k,0}\rho_k + g_k(P_k)$, we get: $m_ke_k = a_{k,0}m_k + \alpha_k g_k(P_k)$ for $k = 1,2$. Thus, multiplying (41) by $a_{k,0}$, and substracting the resulting equation to the energy equation, we get:

$$\begin{array}{l} h_i\epsilon_i\left((\alpha_k g_k(P_k))_i^{n+1} - g_k(P_0)(\alpha_k)_i^n\right) \\ -\frac{1}{2}\Delta t^n g_k(P_0)\left(r_{i+1/2}^n\hat{\epsilon}_{i+1/2}((\alpha_k)_{i+1}^n - (\alpha_k)_i^n) - r_{i-1/2}^n\hat{\epsilon}_{i-1/2}((\alpha_k)_i^n - (\alpha_k)_{i-1}^n)\right) = 0 \end{array} \tag{44}$$

Hence, multiplying (40) by $\epsilon_i g_k(P_0)$ and substracting the result to (44), we get:

$$(\alpha_k)_i^{n+1}\left((g_k(P_k))_i^{n+1} - g_k(P_0)\right) = 0$$

which provides the expected result for all i:

$$(P_k)_i^{n+1} = P_0 \tag{45}$$

This completes the proof for scheme MR.

2. Scheme WBR preserves the discrete form of the basic solution S_2 on any mesh

The scheme WBR ensures that we have: $(\alpha_2)^n_{i+1/2,-} = (\alpha_2)^n_{i+1}$, $(\alpha_2)^n_{i-1/2,+} = (\alpha_2)^n_{i-1}$. Moreover, due to the fact that $(U_k)^n_i = 0$, we get : $(U_k)^n_{i+1/2,-} = (U_k)^n_{i-1/2,+} = 0$, and thus: $(\rho_k)^n_{i+1/2,-} = (\rho_k)^n_{i+1}$, $(\rho_k)^n_{i-1/2,+} = (\rho_k)^n_{i-1}$, together with: $(s_k)^n_{i+1/2,-} = (s_k)^n_{i+1}$, $(s_k)^n_{i-1/2,+} = (s_k)^n_{i-1}$. As a consequence, we get: $(P_k)^n_{i+1/2,-} = (P_k)^n_{i+1} = P_0$, and $(P_k)^n_{i-1/2,+} = (P_k)^n_{i-1} = P_0$. Hence, the discrete equations for the void fraction, the partial masses and the momentum can be simplified, which yields:

$$h_i\left((\alpha_k)^{n+1}_i - (\alpha_k)^n_i\right) - \tfrac{1}{2}\Delta t^n\left((r_{WB})^n_{i+1/2}((\alpha_k)^n_{i+1} - (\alpha_k)^n_i) - (r_{WB})^n_{i-1/2}((\alpha_k)^n_i - (\alpha_k)^n_{i-1})\right) = 0 \quad (46)$$

$$h_i\left((m_k)^{n+1}_i - (m_k)^n_i\right) - \tfrac{1}{2}\Delta t^n\left((r_{WB})^n_{i+1/2}((m_k)^n_{i+1} - (m_k)^n_i) - (r_{WB})^n_{i-1/2}((m_k)^n_i - (m_k)^n_{i-1})\right) = 0 \quad (47)$$

$$h_i\left((m_kU_k)^{n+1}_i - (m_kU_k)^n_i\right) = 0 \quad (48)$$

and eventually:

$$(U_k)^{n+1}_i = 0 \quad (49)$$

We still use the EOS in agreement with: $\rho_k e_k(P_k, \rho_k) = a_{k,0}\rho_k + g_k(P_k)$. Initial conditions are such that the discrete energy equation reduces to:

$$\begin{array}{ll} h_i & \left((m_ke_k)^{n+1}_i - (m_ke_k)^n_i\right) \\ & -\tfrac{1}{2}\Delta t^n\left((r_{WB})^n_{i+1/2}((m_ke_k)^n_{i+1} - (m_ke_k)^n_i) - (r_{WB})^n_{i-1/2}((m_ke_k)^n_i - (m_ke_k)^n_{i-1})\right) = 0 \end{array} \quad (50)$$

Once again, we multiply (47) by $a_{k,0}$ (respectively (46) by $g_k(P_0)$), and substract both to (50). We get:

$$(\alpha_k)^{n+1}_i\left((g_k(P_k))^{n+1}_i - g_k(P_0)\right) = 0$$

which implies that for all i:

$$(P_k)^{n+1}_i = P_0$$

.

C. Property 7

We assume that $\epsilon_L \neq \epsilon_R$, and also that the initial condition (W_L, W_R) of the Riemann problem complies with :

$$I^0_k(W_L) = I^0_k(W_R) \quad (51)$$

The initial condition complies with:

$$\left\{\begin{array}{ll} W^n_i = W_L & pour \quad i \leq j \\ W^n_i = W_R & pour \quad i > j \end{array}\right. \quad (52)$$

We wish to prove that $W^{n+1}_i = W^n_i$ whatever i is. We only foccus on the interface separating cells j and $j+1$.

The assumption (51) implies that:

$$(\alpha_k)^n_j = (\alpha_k)^n_{j+1} \quad (53)$$

and this is of course true for other cells so that $(\alpha_k)^n_{i-1} = (\alpha_k)^n_i = (\alpha_k)^n_{i+1}$. As a consequence, we have $(\alpha_2)^n_{j+1/2,-} = (\alpha_2)^n_{j+1} = (\alpha_2)^n_j$, and $(\alpha_2)^n_{j-1/2,+} = (\alpha_2)^n_{j-1} = (\alpha_2)^n_j$ The discrete equation for the void fraction thus yields:

$$(\alpha_k)^{n+1}_i = (\alpha_k)^n_i \quad \forall i \quad (54)$$

The WBR scheme also enforces that:

$$(\epsilon\alpha_k\rho_kU_k)^n_{j+1/2,-} = (\epsilon\alpha_k\rho_kU_k)^n_{j+1} \quad (55)$$

and thus:

$$(\epsilon)_j(\alpha_k\rho_k U_k)^n_{j+1/2,-} = (\epsilon)_{j+1}(\alpha_k\rho_k U_k)^n_{j+1} \tag{56}$$

The assumption (51) enables to state that:

$$\epsilon_{j+1}(\alpha_k\rho_k U_k)^n_{j+1} = \epsilon_j(\alpha_k\rho_k U_k)^n_j \tag{57}$$

Relations (56), (57) and (54) lead to:

$$(\rho_k)^n_{j+1/2,-}(U_k)^n_{j+1/2,-} = (\rho_k)^n_j(U_k)^n_j \tag{58}$$

A similar work with Riemann invariants s_k and h_k gives:

$$(s_k)^n_{j+1/2,-} = (s_k)^n_{j+1} = (s_k)^n_j \tag{59}$$

$$h_k((\rho_k)^n_{j+1/2,-},(U_k)^n_{j+1/2,-},(s_k)^n_{j+1/2,-}) = h_k((\rho_k)^n_{j+1},(U_k)^n_{j+1},(s_k)^n_{j+1}) = h_k((\rho_k)^n_j,(U_k)^n_j,(s_k)^n_j) \tag{60}$$

Since the scheme WBR retains the solution which is in the same sonic regime, we may conclude, using constraints (59) and (60), that:

$$\begin{cases} (\rho_k)^n_{j+1/2,-} = (\rho_k)^n_j \\ (U_k)^n_{j+1/2,-} = (U_k)^n_j \end{cases} \tag{61}$$

Using a similar process, we also have on the left side of cell j:

$$\begin{cases} (\rho_k)^n_{j-1/2,+} = (\rho_k)^n_j \\ (U_k)^n_{j-1/2,+} = (U_k)^n_j \end{cases} \tag{62}$$

and

$$(s_k)^n_{j-1/2,+} = (s_k)^n_j \tag{63}$$

Inserting previous results (59), (61), (62) and (63) in the scheme WBR implies (for all i):

$$\begin{cases} (m_k)^{n+1}_i = (m_k)^n_i \\ (m_kU_k)^{n+1}_i = (m_kU_k)^n_i \\ (E_k)^{n+1}_i = (E_k)^n_i \end{cases} \tag{64}$$

Hence WBR complies with property 7.

D. Property 8

1. R scheme

Starting with (18) we may rewrite it as:

$$\begin{aligned}(\alpha_2)^{n+1}_i = \left(1-\frac{\Delta t^n}{2h_i}(r^n_{i+1/2}+r^n_{i-1/2})\right)(\alpha_2)^n_i &+\frac{\Delta t^n}{2h_i}\left(r^n_{i+1/2}-(V_I)^n_i\right)(\alpha_2)^n_{i+1} \\ &+\frac{\Delta t^n}{2h_i}\left(r^n_{i-1/2}+(V_I)^n_i\right)(\alpha_2)^n_{i-1}\end{aligned} \tag{65}$$

If the following CFL constraint holds:

$$\frac{\Delta t^n}{2h_i}(r^n_{i+1/2}+r^n_{i-1/2}) \le 1 \qquad \forall i \tag{66}$$

the Rusanov scheme R obviously preserves positive values for α_2. Moreover, noting that (65) remains unchanged when changing α_2 into $1-\alpha_2$, we also conclude that α_1 remains positive under the same CFL condition. Eventually, starting from (19) and using numerical flux definition (20), discrete values of m_k comply with:

$$\begin{aligned}(m_k)^{n+1}_i = \left(1-\frac{\Delta t^n}{2h_i}(r^n_{i+1/2}+r^n_{i-1/2})\right)(m_k)^n_i &+\frac{\Delta t^n}{2h_i}\frac{\epsilon_{i+1}}{\epsilon_i}\left(r^n_{i+1/2}-(U_k)^n_{i+1}\right)(m_k)^n_{i+1} \\ &+\frac{\Delta t^n}{2h_i}\frac{\epsilon_{i-1}}{\epsilon_i}\left(r^n_{i-1/2}+(U_k)^n_{i-1}\right)(m_k)^n_{i-1}\end{aligned} \tag{67}$$

Since $(m_k)^n_i > 0$ for all i, partial masses also remain positive provided that the CFL condition (66) holds.

2. MR scheme

We assume here that: $(\hat{\epsilon})_{i+1/2} = max(\epsilon_i, \epsilon_{i+1})$. Following (22), the governing equation for the void fraction α_2 in scheme MR reads:

$$\begin{aligned}(\alpha_2)_i^{n+1} = \left(1 - \frac{\Delta t^n}{2h_i}\left(\frac{(\hat{\epsilon})_{i+1/2}}{\epsilon_i} r^n_{i+1/2} + \frac{(\hat{\epsilon})_{i-1/2}}{\epsilon_i} r^n_{i-1/2}\right)\right)(\alpha_2)_i^n \quad &+ \frac{\Delta t^n}{2h_i}\left(\frac{(\hat{\epsilon})_{i+1/2}}{\epsilon_i} r^n_{i+1/2} - (V_I)_i^n\right)(\alpha_2)_{i+1}^n \\ &+ \frac{\Delta t^n}{2h_i}\left(\frac{(\hat{\epsilon})_{i-1/2}}{\epsilon_i} r^n_{i-1/2} + (V_I)_i^n\right)(\alpha_2)_{i-1}^n\end{aligned} \tag{68}$$

and the counterpart for the partial mass m_k is:

$$\begin{aligned}(m_k)_i^{n+1} = \quad &\left(1 - \frac{\Delta t^n}{2h_i}\left(\frac{(\hat{\epsilon})_{i+1/2}}{\epsilon_i} r^n_{i+1/2} + \frac{(\hat{\epsilon})_{i-1/2}}{\epsilon_i} r^n_{i-1/2}\right)\right)(m_k)_i^n \\ &+ \frac{\Delta t^n}{2h_i}\frac{(\epsilon)_{i+1}}{(\epsilon)_i}\left(\frac{(\hat{\epsilon})_{i+1/2}}{\epsilon_{i+1}} r^n_{i+1/2} - (U_k)^n_{i+1}\right)(m_k)^n_{i+1} \\ &+ \frac{\Delta t^n}{2h_i}\frac{(\epsilon)_{i-1}}{(\epsilon)_i}\left(\frac{(\hat{\epsilon})_{i-1/2}}{\epsilon_{i-1}} r^n_{i-1/2} + (U_k)^n_{i-1}\right)(m_k)^n_{i-1}\end{aligned} \tag{69}$$

Owing to inequalities $1 \leq \frac{(\hat{\epsilon})_{i+1/2}}{\epsilon_{i+1}}$ and $1 \leq \frac{(\hat{\epsilon})_{i+1/2}}{\epsilon_i}$, the CFL condition:

$$\frac{\Delta t^n}{2h_i}\left(\frac{(\hat{\epsilon})_{i+1/2}}{\epsilon_i} r^n_{i+1/2} + \frac{(\hat{\epsilon})_{i-1/2}}{\epsilon_i} r^n_{i-1/2}\right) \leq 1 \qquad \forall i \tag{70}$$

guarantees that both $(\alpha_2)_i^{n+1}$ and $(m_k)_i^{n+1}$ remain positive, assuming that associated initial values are positive. A similar remark as made above enables to conclude that $(\alpha_2)_i^{n+1} \leq 1$.

3. WBR scheme

We recall first that $max(|(U_k)^n_{i+1/2,-}|, |(U_k)^n_{i+1/2,+}|) \leq (r_{WB})^n_{i+1/2}$. The governing equation for the discrete values of α_2 is exactly the same as the one occuring in the R scheme. Thus, the CFL condition is the same as above and reads:

$$\frac{\Delta t^n}{2h_i}((r_{WB})^n_{i+1/2} + (r_{WB})^n_{i-1/2}) \leq 1 \qquad \forall i \tag{71}$$

We turn now to the discrete partial masses. Starting with (26) and using numerical fluxes of WBR as defined in (27), m_k satisfies:

$$\begin{aligned}(m_k)_i^{n+1} = \quad &\left(1 - \frac{\Delta t^n}{2h_i}((r_{WB})^n_{i+1/2} + (r_{WB})^n_{i-1/2})\right)(m_k)_i^n \\ &+ \frac{\Delta t^n}{2h_i}\left((r_{WB})^n_{i+1/2} - (U_k)^n_{i+1/2,-}\right)(\alpha_k)^n_{i+1}(\rho_k)^n_{i+1/2,-} \\ &+ \frac{\Delta t^h}{2h_i}\left((r_{WB})^n_{i-1/2} + (U_k)^n_{i-1/2,+}\right)(\alpha_k)^n_{i-1}(\rho_k)^n_{i-1/2,+}\end{aligned} \tag{72}$$

Owing to the definition of $(r_{WB})^n_{i+1/2}$, $(m_k)_i^{n+1}$ is clearly a convex combination of the discrete partial mass $(m_k)_i^n$, and discrete densities $(\rho_k)^n_{i+1/2,-}$ and $(\rho_k)^n_{i-1/2,+}$, which are positive, provided that:

$$\frac{\Delta t^n}{2h_i}((r_{WB})^n_{i+1/2} + (r_{WB})^n_{i-1/2}) \leq 1 \tag{73}$$

.

XI. Appendix C : Computing the interface states of WBR scheme

We first provide below the main guidelines to compute the interface state $Z^n_{i+1/2,-}$, assuming of course that $\epsilon_i\epsilon_{i+1} \neq 0$. Components of $Z^n_{i+1/2,-}$ should agree with :

$$Inv^0_m(Z^n_{i+1/2,-}, \epsilon_i) = Inv^0_m(Z^n_{i+1}, \epsilon_{i+1})$$

As a consequence, we have $(\alpha_k)^n_{i+1/2,-} = (\alpha_k)^n_{i+1}$, $(s_k)^n_{i+1/2,-} = (s_k)^n_{i+1}$ and:

$$\epsilon_i(\alpha_k)^n_{i+1/2,-}(\rho_k)^n_{i+1/2,-}(U_k)^n_{i+1/2,-} = \epsilon_{i+1}(\alpha_k)^n_{i+1}(\rho_k)^n_{i+1}(U_k)^n_{i+1}$$

$$2h_k((s_k)^n_{i+1/2,-},(\rho_k)^n_{i+1/2,-}) + ((U_k)^n_{i+1/2,-})^2 = 2h_k((s_k)^n_{i+1},(\rho_k)^n_{i+1}) + ((U_k)^n_{i+1})^2$$

where : $\rho_k h_k(s_k,\rho_k) = \rho_k e_k(P_k(s_k,\rho_k),\rho_k) + P_k(s_k,\rho_k)$. Setting as the main unknown $X = (\rho_k)^n_{i+1/2,-}$, and substituting in the last equation, one needs to solve :

$$\psi^n_{i+1/2,-}(X) = 0 \tag{74}$$

where :

$$\psi^n_{i+1/2,-}(X) \stackrel{def}{=} 2\left(h_k((s_k)^n_{i+1},X) - h_k((s_k)^n_{i+1},(\rho_k)^n_{i+1})\right) + ((U_k)^n_{i+1})^2\left(\frac{(\epsilon_{i+1}(\rho_k)^n_{i+1})^2}{(\epsilon_i X)^2} - 1\right) \tag{75}$$

The solution is obviously $X = (\rho_k)^n_{i+1}$ when $\epsilon_i = \epsilon_{i+1}$. If $\epsilon_i \neq \epsilon_{i+1}$, we proceed as follows:

- If $(U_k)^n_{i+1} = 0$, the solution of (74) is $X = (\rho_k)^n_{i+1}$.
- Otherwise, one first computes $X_{min} > 0$ solution of :

$$X^3_{min}\left(\partial_{\rho_k}\left(h_k(s_k,\rho_k)\right)\right)((s_k)^n_{i+1},X_{min}) = \left(\frac{(U_k)^n_{i+1}\epsilon_{i+1}(\rho_k)^n_{i+1}}{\epsilon_i}\right)^2 > 0 \tag{76}$$

  The following two possibilities arise:

  – Either:

  $$\psi^n_{i+1/2,-}(X_{min}) > 0$$

  In that case, (74) has no solution. The computation is stopped. Another alternative consists in setting the solution to X_{min}.

  – Otherwise, the equation (74) admits two solutions $X^- \in]0, X_{min}]$ and $X^+ \in [X_{min}, +\infty[$. The final solution is $X = X^-$ if $(\rho_k)^n_{i+1} \leq X_{min}$, and $X = X^+$ if $X_{min} \leq (\rho_k)^n_{i+1}$.

$Z^n_{i+1/2,+}$ is obtained with a similar way, using $(\rho_k)^n_i$ to determine the admissible branch of solutions.

References

[0] Ambroso A., Chalons C. , Coquel F., Godlewski E. , Lagoutière F., Raviart P. A., Seguin N., Working group on the interfacial coupling of models, http://www.ann.jussieu.fr/groupes/cea.

[1] Andrianov N., Warnecke G., "the Riemann problem for the Baer-Nunziato two-phase flow model " *J. Comput. Physics*, vol. 195, pp. 434-464 , 2004.

[2] Audusse E., Bouchut F., Bristeau M.O., Klein R., Perthame B., "A fast and stable well-balanced scheme with hydrodynamic reconstruction for shallow water flows" *SIAM J. Sci. Comput.*, vol. 25, pp. 2050-2065, 2004.

[3] Baer M.R., Nunziato J.W., "A two-phase mixture theory for the deflagration to detonation transition (DDT) in reactive granular materials", *Int. J. Multiphase Flow*, vol. 12(6), pp. 861–889, 1986.

[4] Bouchut F., *"Nonlinear stability of Finite Volume methods for hyperbolic conservation laws, and well-balanced schemes for sources"*, Frontiers in Mathematics series, Birkhauser, 2004.

[5] Boutin B., Coquel F., Godlewski E., "The Dafermos regularization for the interface coupling of conservation laws", Hyperbolic problems: Theory, Numerics, Applications, Springer, pp. 567-575, 2008.

[6] Buffard T., Gallouët T., Hérard J.-M., "A sequel to a rough Godunov scheme. Application to real gases ", *Computers and Fluids*, vol. 29(7), pp. 813-847, 2000.

[7] Chinnayya A., Le Roux A.Y., Seguin N. , "A well-balanced numerical scheme for shallow-water equations with topography: the resonance phenomena", *Int. J. Finite Volumes (electronic)*, http://www.latp.univ-mrs.fr/IJFV/, vol. 1(1), 2004.

[8] Coquel F., Gallouët T., Hérard J.M., Seguin N., "Closure laws for a two-fluid two-pressure model", *C. R. Acad. Sci. Paris*, vol. I-332, pp. 927–932, 2002.

[9] Eymard R., Gallouët T., Herbin R., "*Finite Volume methods*", in Handbook of Numerical Analysis, P.G. Ciarlet and J.L. Lions editors, North Holland, vol. VII, pp. 715-1022, 2000.

[10] Gallouët T., Hérard J.-M., Seguin N., "A hybrid scheme to compute contact discontinuities in one dimensional Euler systems", *Math. Model. and Numer. Anal.*, vol. 36, pp. 1133-1159, 2002.

[11] Gallouët T., Hérard J.-M., Seguin N., "Some recent Finite Volume schemes to compute Euler equations using real gas EOS", *Int. J. Num. Meth. Fluids*, vol. 39, pp.1073-1138, 2002.

[12] Gallouët T., Hérard J.-M., Seguin N., "Some approximate Godunov schemes to compute shallow water equations with topography ", *Computers and Fluids*, vol.32(3), pp. 479-513, 2003.

[13] Gallouët T., Hérard J.-M., Seguin N., "Numerical modelling of two phase flows using the two-fluid two-pressure approach", *Math. Mod. Meth. in Appl. Sci.*, vol. 14(5), pp. 663-700, 2004.

[14] Girault L., Hérard J.-M., "Multidimensional computations of a two-fluid hyperbolic model in a porous medium", *AIAA paper 2009-3540*, http://www.aiaa.org, 2009.

[15] Goatin P., Le Floch P., "The Riemann problem for a class of resonant hyperbolic systems of balance laws", *Annales Inst. Henri Poincare*, vol. 21(6), pp. 881-902, 2004

[16] Godlewski E., "Coupling fluid models. Exploring some features of interfacial coupling", *Invited paper, in the proceedings of Finite Volumes for Complex Applications V*, Aussois, France, June 8-13, 2008 .

[17] Godlewski E., Raviart P.A., "The numerical interface coupling of nonlinear hyperbolic systems of conservation laws: 1.The scalar case", *Numerische Mathematik*, vol. 97, pp. 81-130, 2004.

[18] Godlewski E., Le Thanh K.C., Raviart P.A., "The numerical interface coupling of nonlinear hyperbolic systems of conservation laws: 2. The case of systems", *Math. Mod. Num. Anal.*, vol. 39, pp. 649-692, 2005.

[19] Godunov S.K., "Finite difference method for numerical computation of discontinuous solutions of the equations of fluid dynamics", *Mat. Sb.*, vol. 47, pp. 271-300, 1959.

[20] Greenberg J.M., Leroux A.Y., "A well balanced scheme for the numerical processing of source terms in hyperbolic equations", *SIAM J. Num. Anal.*, vol. 33(1), pp. 1–16, 1996.

[21] Guillemaud V., "Modélisation et simulation numérique des écoulements diphasiques par une approche bifluide à deux pressions", *P*hD thesis, Université Aix Marseille I, Marseille, France, 27th of March, 2007.

[22] Helluy P., Hérard J.-M., Mathis H., "A well-balanced approximate Riemann solver for variable cross-section compressible flows", *AIAA paper 2009-3888*, http://www.aiaa.org, 2009.

[22] Hérard J.M. , "A rough scheme to couple free and porous media", *Int. J. Finite Volumes (electronic)*, http://www.latp.univ-mrs.fr/IJFV/, vol. 3(2), pp. 1-28, 2006.

[23] Hérard J.-M., "A three-phase flow model", *Mathematical Computer Modelling*, vol. 45, pp. 432-455, 2007.

[24] Hérard J.-M., "Un modèle hyperbolique diphasique bi-fluide en milieu poreux", *CRAS Mécanique*, vol. 336, pp. 650-655, 2008.

[25] Kapila A.K., Son S.F., Bdzil J.B., Menikoff R., Stewart D.S., "Two-phase modeling of a DDT: structure of the velocity relaxation zone", *Phys. of Fluids*, vol. 9(12), pp. 3885–3897, 1997.

[26] Kröner D., Le Floch P., Thanh M.D., "The minimum entropy principle for compressible fluid flows in a nozzle with discontinuous cross section", *Math. Mod. Num. Anal.* , vol. 42(3), pp. 425-443, 2008.

[27] Kröner D. , Thanh M.D., "Numerical solution to compressible flows in a nozzle with variable cross-section", *SIAM J. Numer. Anal.* , vol. 43(2), pp. 796–824, 2006.

[28] Lowe C.A., "Two-phase shock-tube problems and numerical methods of solution " *J. Comput. Physics*, vol. 204, pp. 598-632, 2005.

[29] Schwendeman D.W., Wahle C.W., Kapila A.K., "The Riemann problem and a high resolution Godunov method for a model of compressible two-phase flow" *J. Comput. Physics*, vol. 212, pp. 490-526, 2006.